Seismicity during continental breakup in the Red Sea rift of Northern Afar

Finnigan Illsley-Kemp[1], Derek Keir[1,2], Jonathan M. Bull[1], Thomas M. Gernon[1], Cynthia Ebinger[3], Atalay Ayele[4], James O. S. Hammond[5], J-Michael Kendall[6], Berhe Goitom[6] and Manahloh Belachew[7]

[1]National Oceanography Centre Southampton, University of Southampton, Southampton, United Kingdom [2]Dipartimento di Scienze della Terra, Università degli Studi di Firenze, Florence, Italy [3]Department of Earth and Environmental Sciences, Tulane University, New Orleans, USA [4]Institute of Geophysics Space Science and Astronomy, Addis Ababa University, Addis Ababa, Ethiopia [5]Department of Earth and Planetary Sciences, Birkbeck, University of London, London, United Kingdom [6]School of Earth Sciences, University of Bristol, Bristol, United Kingdom, [7]Boone Pickens School of Geology, Oklahoma State University, Stillwater, USA

Key Points:

- Seismicity in Northern Afar is focused at the rift axis and western rift margin.
- Low-frequency seismicity at the rift axis shows evidence for a ~12 km deep magma complex.
- Seismicity at the western rift margin is caused by faulting associated with enhanced crustal thinning or crustal flexure.

Abstract

Continental rifting is a fundamental component of plate tectonics. Recent studies have highlighted the importance of magmatic activity in accommodating extension during late-stage rifting, yet the mechanisms by which crustal thinning occurs are less clear. The Red Sea rift in Northern Afar presents an opportunity to study the final stages of continental rifting as these active processes are exposed sub-aerially. Between February 2011 and February 2013 two seismic networks were installed in Ethiopia and Eritrea. We locate 4951 earthquakes, classify them by frequency content and calculate 31 focal mechanisms. Results show that seismicity is focused at the rift axis and the western marginal graben. Rift axis seismicity accounts for ~64% of the seismic moment release and exhibits a swarm-like behavior. In contrast, seismicity at the marginal graben is characterized by high-frequency earthquakes that occur at a constant rate. Results suggest that the rift axis remains the primary locus of seismicity. Low frequency earthquakes, indicative of magmatic activity, highlight the presence of a magma complex ~12 km beneath Alu-Dalafilla at the rift axis. Seismicity at the marginal graben predominantly occurs on westward dipping, antithetic faults. Focal mechanisms show that this seismicity is accommodating E-W extension. We suggest

This article has been accepted for publication and undergone full peer review but has not been through the copyediting, typesetting, pagination and proofreading process which may lead to differences between this version and the Version of Record. Please cite this article as doi: 10.1002/2017JB014902

that the seismic activity at the marginal graben is either caused by upper crustal faulting accommodating enhanced crustal thinning beneath Northern Afar, or as a result of flexural faulting between the rift and plateau. This seismicity is occurring in conjunction with magmatic extension at the rift axis, which accommodates the majority of long-term extension.

1 Introduction

The breakup of continents to form ocean basins is a fundamental process in plate tectonic Wilson Cycles, however the processes governing the transition from continental rifting to seafloor spreading have largely remained enigmatic. In particular, it is unclear how crustal extension is accommodated and whether it predominantly occurs through mechanical faulting of the crust or magmatic activity. Studies of developed continental rifts have shown that as continental rifting progresses to breakup, extension is increasingly accommodated by magmatism [*Wolfenden et al.*, 2005]. Localized magmatism serves to focus extension at the rift axis through dyking and lower crustal sill intrusions [*Buck*, 1991; *Ebinger et al.*, 2013; *Mackenzie et al.*, 2005; *Thybo and Nielsen*, 2009]. Further, numerical models demonstrate that magmatic activity plays an important role in strain localization from rift onset to plate rupture [e.g., *Buck*, 2004; *Bialas et al.*, 2010; *Allken et al.*, 2012]. However, the role that mechanical faulting and seismicity play in the final stages of continental rifting remain poorly understood, in large part because the process is occurring in only a few remote areas worldwide [e.g., *Bosworth et al.*, 2005; *Bastow and Keir*, 2011; *Persaud et al.*, 2016].

Most studies of continental breakup rely on data from passive margins that have undergone full continental breakup. Although 2D, and in some cases, 3D details of crustal structures can be gained from such studies [e.g., *White and McKenzie*, 1989; *Pindell et al.*, 2014; *Quirk et al.*, 2014], the thermal and mechanical response of the lithosphere to stretching is obscured by thick sedimentary and volcanic sequences, and the thermal processes have long since decayed. To counter this problem, studies of currently active continental rifts and young ocean basins can provide solutions to questions regarding the distribution and accommodation of extension during rifting.

The Southern Red Sea rift in the Danakil Depression of Northern Afar, Ethiopia/Eritrea, provides a unique opportunity to document processes occurring during continental breakup (Figure 1). The Danakil Depression is currently undergoing the final stages of continental breakup in an area affected by magmatism since rift onset [*Wolfenden et al.*, 2005; *Medynski et al.*, 2013; *Stab et al.*, 2016]. For two years, from 2011 to 2013, we deployed a seismic network of fifteen stations in the Danakil region, which was combined with a network of six stations deployed in Eritrea during the same time period (Figure 2). We use the continuous seismic data to identify the spatial distribution of brittle deformation within the crust, its depth extent, and its frequency content to shed new light on the rifting cycle.

2 Tectonic Background

2.1 The Afar Depression

The Afar Depression marks a triple junction between the Arabian, Somalian and Nubian plates, and contains the narrow Danakil microplate [*McKenzie and Davies*, 1970; *Mohr*, 1970; *Tesfaye et al.*, 2003; *DeMets and Merkouriev*, 2016] (Figure 1). Geochronological results suggest that rifting between Arabia and Africa began ~ 29 − 31 Ma with extension focused on large scale (>50 km) border faults [*Ayalew et al.*, 2006; *Wolfenden et al.*, 2005], which now separate the substantial 2–3 km high Ethiopian and Southeastern plateaus from the Afar Depression, which reaches ~100 m below sea level. Further to the south lies the younger, Main Ethiopian Rift (MER), where E-W extension is oblique to the NE-SW directed extension in the southern Red Sea and Gulf of Aden [e.g., *Bendick et al.*, 2006]. The MER initiated at ~18 Ma, with initial strain localized along long, large offset border faults [*Ebinger et al.*, 1993].

Extension in the MER has, since the Quaternary, migrated away from the basin bounding border faults and has localized to rift-aligned magmatic segments at the rift axis [*Wolfenden et al.*, 2004]. Here extension is accommodated through dyking and magmatic underplating processes which mask the total crustal thinning [*Mackenzie et al.*, 2005]. A similar such migration of extension occurred in the southern Red Sea rift between 25 and 20 Ma [*Hayward and Ebinger*, 1996; *Wolfenden et al.*, 2005; *Stab et al.*, 2016]. This migration of extension is characterized by a focusing of magmatism and faulting at the rift axis and has been postulated to be the final stage of continental rifting, prior to the transition to seafloor spreading.

GPS measurements from northern Afar show that extension is currently oriented NE-SW [*McClusky et al.*, 2010] (Figure 2). In the southern Danakil Depression, extension rates are ~20 mm/yr, decreasing to the north until extension is transferred entirely to the Red Sea rift in the northeast [*McClusky et al.*, 2010]. Active deformation studies also indicate that strain is localized to ~50 km long, <20 km wide zones of Quaternary-Recent magma intrusion and faulting, referred to as magmatic segments [*Casey et al.*, 2006]. Northern Afar features large changes in topography and crustal thickness. The crust beneath the Ethiopian Plateau is ~40 km thick, but thins dramatically eastward to ~20-26 km beneath the ~300 m wide Afar Depression [*Hammond et al.*, 2011]. The crust beneath the Danakil Depression is ~15 km thick, suggesting ongoing, crustal thinning and magma intrusion [*Bastow and Keir*, 2011; *Hammond et al.*, 2011; *Makris and Ginzburg*, 1987; *Tiberi et al.*, 2005]. Geophysical surveys have shown that the crust beneath the Danakil Depression has seismic velocities that are consistent with stretched and heavily intruded continental crust, with V_P/V_S ratios of >1.9 strongly suggesting the presence of partial melt in the crust [*Hammond et al.*, 2011; *Dugda et al.*, 2005; *Makris and Ginzburg*, 1987; *Tiberi et al.*, 2005].

Global and regional studies of seismic tomography show a broad low-velocity

anomaly rising from 400 to 50 km beneath East Africa and the southern Red Sea [*Ritsema et al.*, 2011; *Chang and Van der Lee*, 2011; *Hansen et al.*, 2012]. These observations are taken to represent a broad thermal upwelling known as the African Superplume. More detailed tomographic imaging of the Main Ethiopian and Afar rifts and their uplifted flanks using local seismic networks show that there are markedly lower velocities beneath the rift valleys, consistent with the presence of partial melt [*Bastow et al.*, 2008; *Hammond et al.*, 2013; *Stork et al.*, 2013; *Civiero et al.*, 2015, 2016]. In addition, *Gallacher et al.* [2016] suggest that melt generation in the asthenospheric mantle beneath the Afar Depression is segmented and buoyancy-driven, resembling characteristics of the mantle beneath regions of seafloor spreading [e.g., *Wang et al.*, 2009; *Ligi et al.*, 2012]. The observations from broadband seismology corroborate geochemical models which suggest an elevated mantle potential temperature of 1450° C [*Ferguson et al.*, 2013; *Armitage et al.*, 2015].

2.2 The Danakil Depression

The Danakil Depression is situated in the northernmost Afar Depression and is a ~200 km long 50–150 km wide basin (Figure 2). It is bounded to the west by ~3 km of relief, controlled by an Oligo-Miocene border fault system; to the east it is bounded by the Danakil block, a narrow horst of crystalline basement and Miocene sediments which forms 500–1000 m of elevation.

The western rift-margin is characterized by narrow (10–20 km wide) marginal grabens which lie at the foot of the Oligo-Miocene border faults [*Tesfaye et al.*, 2003; *Wolfenden et al.*, 2005; *Stab et al.*, 2016]. These marginal grabens extend from the intersection of the MER and Red Sea rift at ~10°N to the northern Danakil Depression, yet they are not found within the MER [*Tesfaye et al.*, 2003]. *Wolfenden et al.* [2005] and *Tesfaye et al.* [2003] observed that between 10°N and 11°N the marginal grabens are composed of both ENE and WSW dipping normal faults. However, further north at ~11.5°N *Stab et al.* [2016] do not observe any ENE dipping faults and instead find that faults consistently dip WSW, antithetic to the Oligo-Miocene border faults. Through dating of sedimentary and volcanic sequences, *Wolfenden et al.* [2005] found that displacement on the marginal graben faults postdates 14 Ma and thus are an exception to the general pattern of rift migration of extension. *Wolfenden et al.* [2005] suggests that the marginal grabens are formed through crustal flexure due to the discrepancy between crustal thickness and density between the thick, felsic plateau and the thin, highly intruded crust in the Afar Depression. Alternatively, *Stab et al.* [2016] propose that the WSW dipping faults of the marginal grabens are the surface manifestation of antithetic mid-crustal shear zones.

The Danakil Depression lies predominantly below sea level but is currently subaerial, with the surface geology dominated by thick layers of evaporites, formed during repeated marine incursions. In addition there are abundant basaltic lavas from the Erta-Ale magmatic segment, which is the focus for the majority of Quaternary to Recent volcanism in Afar [*Barberi and Varet*, 1970; *Bastow and Keir*, 2011; *Keir et al.*, 2013]. At the southern end of the Danakil Depression lies the seismically active

Tat-Ale volcanic range [*Barberi and Varet*, 1970; *Belachew et al.*, 2011]. The Erta-Ale and Tat-Ale ranges acts as the locus of plate boundary deformation [*Pagli et al.*, 2014]. Further to the south the rift axis steps en-echelon to the southwest to the Dabbahu-Manda Harraro magmatic segment [*Belachew et al.*, 2011]. Within this step-over region lies the NE-SW trending Alayta range and Afdera volcano and many NE trending faults, which are inferred to open obliquely and promote volcanism [*Barberi and Varet*, 1970; *Belachew et al.*, 2011]. To the east of the Danakil Depression, on the Danakil block, is the Bidu volcanic complex [*Wiart and Oppenheimer*, 2005] which consists of two calderas, Nabro and Mallahle.

The majority of recorded large-magnitude seismicity in the Danakil region occurs at the western rift margin (Figure 2), including a 2002 earthquake swarm near the town of Mekele featuring a M_W 5.6 event [*Ayele et al.*, 2007]. To the south of the Danakil Depression, earthquake monitoring revealed an intense period of seismicity associated with the 2005–2010 Dabbahu-Manda Hararo dyke sequence [*Belachew et al.*, 2011; *Barnie et al.*, 2015]. The dyke intrusions at Dabbahu were associated with low-frequency earthquakes during dyke propagation [*Tepp et al.*, 2016].

The Danakil region has hosted much recent volcanic activity with all magmatic segments, excluding the Tat-Ale volcanic range, featuring earthquakes and caldera and fissure eruptions since historical records began [*Gouin*, 1979; *Wiart and Oppenheimer*, 2005; *Pagli et al.*, 2012]. At Gada-Ale, radar interferometry was used to show that an actively deforming magma chamber exists beneath the volcano [*Amelung et al.*, 2000]. Seismicity and satellite observations were used to show that a 6 x 10^6 m^3 dyke intrusion, sourced from a previously unrecognized magma chamber, occurred at Dallol in 2004 [*Nobile et al.*, 2012]. Similarly, in 2008, a 5.1 × 10^6 m^3 dyke intruded at Alu-Dalafilla and resulted in a fissure eruption that covered an area of ~16 × 10^6 m^2 [*Pagli et al.*, 2012]. In November 2010, the lava lake of Erta-Ale erupted ~6 x 10^6 m^3 of basaltic lava onto the crater floor [*Field et al.*, 2012] and this same volcano underwent another major eruption in January 2017 [*Xu et al.*, 2017]. In 2011, in Eritrea, Nabro volcano underwent a major caldera-style eruption that generated ash clouds reaching 17 km height [*Clarisse et al.*, 2014], an estimated 4.3 Tg of SO_2 [*Theys et al.*, 2013] and a lava flow that stretched for 17.5 km [*Goitom et al.*, 2015; *Hamlyn et al.*, 2014].

3 Data and Methods

3.1 Seismic Data

The seismic network comprised fifteen stations in Ethiopia, active for two years between February 2011 and February 2013. This was supplemented by a network of six stations in Eritrea active between June 2011 and October 2012. The resulting combined network consisted of seventeen Güralp CMG-3ESPCD instruments and four Güralp CMG6TD instruments that all recorded continuous seismic data at 50 Hz. Earthquakes were picked manually for both P and S waves and events were located with NonLinLoc [*Lomax et al.*, 2000]. We used a two-dimensional velocity model

based on controlled source experiments and receiver functions [*Hammond et al.*, 2011; *Makris and Ginzburg*, 1987]. This resulted in a total of 4951 earthquakes in a catalog complete above magnitude 2.0, where magnitudes are calculated using a region-specific local magnitude scale [*IllsleyKemp et al.*, 2017a]. In Figure 3 we plot earthquakes with horizontal errors less than ±5 km, amounting to 1429 events.

3.2 Frequency Analysis

We use frequency index, *FI*, to classify earthquakes based on their spectral content. This allows us to probe the source of seismic activity and whether seismicity is influenced by magmatic processes. We use the procedure outlined by *Buurman and West* [2006] who define *FI* as:

$$FI = \log (A_{upper}/A_{lower}), \quad (1)$$

where A_{upper} and A_{lower} are the spectral amplitudes measured across a band of high and low frequencies respectively. Through inspection of the frequency spectrum of characteristic events (Figure 4) we define the low frequency band as 0.5–2 Hz and the high frequency band as 7–11 Hz, following the strategy of *Tepp et al.* [2016]. We then calculate *FI* for further calibration events at each station, in order to test whether the *FI* method can distinguish between different types of events or a continuous spectrum.

Owing to the heterogeneity of surface materials in basins and volcanic ranges and the shallow active faulting in the area, path effects may influence the spectral content [*Coté et al.*, 2010; *McNutt*, 2005; *Tepp et al.*, 2016]. However, the spectral content of P-waves are more sensitive to source effects [*Tepp et al.*, 2016]. We therefore performed the calculation over both the full waveform and short time windows that isolate the P-wave. Figure 5 shows that we see a clear distinction between high frequency, hybrid and low frequency for all stations when using only the P-wave. The distinction becomes less clear when the full waveform is used. We use these results to define the *FI* windows for each station and calculate *FI* values for all earthquakes with a SNR ratio of over 2.5 (Figure 6).

3.3 Earthquake Relocation and Focal Mechanisms

In order to better constrain hypocentral locations we compute relative relocations using the double-difference software HypoDD and a 1D velocity model taken from the model used for absolute locations [*Waldhauser*, 2001]. We use a combination of P and S wave phase picks and cross-correlation derived P-wave differential travel times. The relocation procedure tightens earthquake hypocenters and images active fault planes with much greater accuracy, allowing us to interpret structural features with increased confidence. We relocate the earthquakes occurring at the western marginal graben and successfully relocate 745 events with an average horizontal error of ±0.58 km and average depth error of ±0.58 km (Figure 7). We then compute focal mechanisms based on first-motion P-wave polarities using the HASH software [*Hardebeck and Shearer*, 2002, 2003]. This results in a total of 31 focal mechanisms with solution probabilities >70%. The type of faulting that each focal mechanism

represents is determined by the plunge of the T, B and P axes (Kaverina et al., 1996; Álvarez-Gómez, 2014). This results in 26 of 31 focal mechanisms having normal fault solutions (Figure 8). This is further corroborated by full moment tensors from 2007—2008 (Figure 2). A more detailed discussion of the associated full moment tensor methodology can be found in the supporting information [Dreger et al., 2000; Dreger, 2008; Minson and Dreger, 2008; Saikia, 1994; Belachew et al., 2011; Belachew et al., 2013].

4 Results

To aid discussion of results we divide the earthquake catalogue into three groups; the full catalogue of 4951 earthquakes, earthquakes that had sufficient SNR to be classified using the *FI* method (1191 earthquakes) (Figure 6) and earthquakes relocated with HypoDD (745 earthquakes) (Figure 7). We use the full catalogue to draw interpretations where high-accuracy locations are not necessary, for example when comparing large regions (Figures 9, 11, 12). *FI* classified earthquakes are used to probe potential source mechanisms for seismicity (Figures 6, 10), and relocated earthquakes are used to interpret tectonic structures, where highly-accurate locations are required (Figures 7, 13).

The earthquake locations can be broadly categorized into two groups: seismicity at the rift axis and at the western marginal graben system (Figure 3). The catalogue earthquakes that are focused at the rift axis show a clear along-axis segmentation coinciding with the axial magmatic segments that have been sites of historic and modern eruptions and intrusions. There is a cluster of 54 earthquakes focused at the Dabbahu magmatic segment with magnitudes ranging from 1.0 to 2.8 and a mean depth of 9.1 km. The Dabbahu segment has undergone 14 separate dyke intrusions since a ~60 km long dyke was intruded in 2005 [*Wright et al.*, 2006; *Hamling et al.*, 2009; *Ebinger et al.*, 2008; *Belachew et al.*, 2011], causing similar clusters of rift-aligned seismicity. The SNR at nearby stations was not of high enough quality to perform a frequency analysis to evaluate the spectral content.

The locus of catalogue seismicity then steps en-echelon to the northeast where there is a region of clustered seismicity (562 earthquakes), between the Tat-Ale and Erta-Ale magmatic segments (the Giulietti Plain, Figure 2b). The seismicity here includes some of the largest magnitude events in the region (M_L 4.2) and is characterized by high frequency events (Figure 6). Continuing northward, seismic activity is focused along the Erta-Ale magmatic segment, 885 earthquakes form a rift-aligned pattern with individual clusters at Erta-Ale, Alu-Dalufilla and Dallol. Magnitudes range from 1.1 to 3.9, with the majority of events occurring at shallow depths (<2 km; Figure 11).

There is a particular focus of seismicity at the Alu-Dalafilla volcanic complex; 554 earthquakes occurred beneath the volcano during the study period. Seismicity here exhibits a pulsing swarm-like behaviour with an increase in activity in mid-2012: 368 earthquakes occurred between April 2012 and November 2012 (Figure 9). The majority of the *FI* classified seismicity at Alu-Dalafilla is classified as low-frequency and occurs in a cluster of 29 events at ~12 km depth (Figures 6, 9, 10). The deeper

low-frequency events form a roughly circular structure ~10 km in diameter (Figures 10, 13). The Erta-Ale magmatic segment is responsible for a seismic moment release of ~7×10^{15} Nm during the study period, amounting to ~65% of the total seismic moment release in the region. The seismic moment release at Alu-Dalafilla is dominated by the deep (~12 km) earthquakes (Figure 11).

A large proportion of the catalogue seismicity (1429 events) is focused at the western marginal graben, at the foot of the Oligo-Miocene border fault system (Figure 7). This area has been active historically [*Gouin*, 1979], with the most recent documented earthquake sequence during August, 2002 [*Ayele et al.*, 2007; *Belachew et al.*, 2011]. The rate of seismicity at the western marginal graben does not vary significantly through time (Figure 9) and the *FI* classified earthquakes are almost exclusively high frequency events (Figure 6). Earthquakes are generally focused in the upper 5 km but extend to over 20 km depth in both the full catalogue and relocated earthquakes (Figures 11, 13). Magnitudes here range from 0.36-3.77 M_L. The seismic moment release at the western marginal graben amounts to ~4×10^{15} Nm. Over 80% of the calculated focal mechanisms at the margin represent normal faulting, the majority of which is consistent with extension oriented ENE-WSW. Using the 745 relocated events, seismicity on the margin shows a clear, westward dipping structure, that is antithetic to the dominate dip-direction of the Oligo-Miocene border faults, which dip towards the rift axis. This seismically active structure is oriented roughly N-S and is ~50 km in length (Figure 7).

5 Discussion

Seismic activity at the Erta-Ale magmatic segment accounts for ~64% of the seismic moment release in the Danakil Depression over the period of our study (Figure 12). Although a large proportion of the seismicity occurs at shallow depths (<2 km), a significant amount of activity occurs at ~10–12 km depth (Figure 11). In addition the seismicity rate through time indicates swarm activity with a period of increased seismicity from April 2012 to September 2012 (Figure 9). The seismicity at the Erta-Ale volcanic range is dominated by activity at the Alu-Dalafilla volcanic complex (Figure 3). Through frequency analysis we show that seismicity beneath Alu-Dalafilla features a high proportion of low-frequency earthquakes (Figures 6, 10). Low frequency seismicity typically has a frequency range of 0.5–5 Hz and generally consists of a sudden, broadband onset followed by decaying harmonic signals [*Chouet*, 1996]. Low frequency earthquakes at volcanic systems can be produced by acoustic waves, propagating within a fluid filled crack [*Aki et al.*, 1977; *Chouet*, 1986; *Chouet and Matoza*, 2013]. We therefore interpret that the low frequency earthquakes beneath Alu-Dalafilla are caused by magma movement in a previously unidentified reservoir at ~12 km depth (Figures 10, 13).

Through modelling of ground deformation, *Pagli et al.* [2012] have shown that there is a magma chamber at ~4 km depth beneath Alu-Dalafilla with an associated sill at 1 km depth, which was the source of the 2008 fissure eruption. We propose that the

shallow dyke and sill complex at Alu-Dalafilla are fed by the lower crustal magma reservoir identified in our study. This is likely fed aseismically from the mantle and would suggest a stacked sill reservoir system such as that proposed at Eyjafjallajökull and Bárðarbunga, Iceland [*Sigmundsson et al.,* 2010*; Tarasewicz et al.,* 2012, *Hudson et al*., 2017] and beneath the Dabbahu-Manda-Hararo magmatic segment [*Desissa et al*., 2013, *Hammond*, 2014]. The inferred magma plumbing system is similar to those proposed at slow-spreading ocean ridges [*Carbotte et al., 2013; Jian et al.*, 2017; *Schmid et al.*, 2017]. This suggests that such structures may form during continental rifting and persist through to seafloor spreading. This supports the model proposed by *Gallacher et al.* [2016] that segmented mantle-upwelling, typical of mid-ocean ridges, initiates during continental rifting.

It is interesting to note that we observe very little seismic activity and we detect no low-frequency seismicity beneath Erta-Ale volcano, consistent with previous short-term seismic experiments [*Harris et al.*, 2005; *Jones et al.*, 2012]. Erta-Ale is an extremely active volcano, maintaining a persistent lava lake and hosting frequent eruptions [*Field et al.*, 2012; *Vergniolle and Bouche*, 2016]. Analysis of SO_2 flux, in March 2003, suggest a magma supply rate of 350–650 kg/s [*Oppenheimer et al.*, 2004], however this may not be indicative of the current magma flux. Further, the low form of the basaltic shield complex indicates that it is actively broadening through dyke intrusion. We see no evidence in the seismicity for a magma conduit beneath Erta-Ale (Figure 10). It may be that magma replenishment did not occur during the two-year period of this study, however this seems unlikely given the sustained high supply rate [*Oppenheimer et al.*, 2004]. Another possibility could be that the seismic activity associated with magma replenishment lies below the detection threshold of our catalogue which is complete to magnitude 2.0 M_L [*Illsley-Kemp et al.*, 2017a]. Erta-Ale is an open magmatic system, where changes in magma chamber pressure can be relieved by changes in lava lake level [*Vergniolle and Bouche*, 2016] and it is also likely that the crust beneath Erta-Ale is hot and/or contains a high melt percentage. Both characteristics would inhibit the buildup of stress required for brittle failure, as observed at Askja volcano, Iceland [*Greenfield et al.*, 2016].

While strain continues to be focused at the Erta-Ale magmatic segment the intense seismicity at the western marginal graben marks a distinct change in how strain is distributed in comparison to the rest of Afar and the MER. This pattern of increased seismicity at the western margin of the Danakil Depression is also observed in the 2007–2009 study of *Belachew et al.* [2011] and the National Earthquake Information Centre (NEIC) earthquake catalogue [*Keir et al.,* 2013] (Figure 2). Seismicity at the western marginal graben accounts for ~36% of the seismic moment release in the Danakil Depression (Figure 12). The majority of this seismicity is focused in the upper crust and occurs at a consistent rate through time (Figures 9, 11). This suggests that the seismicity at the western marginal graben is tectonic (i.e. non-volcanic) in origin, and that it accounts for a significant proportion of the deformation in the Danakil Depression. This constitutes a change from the Main Ethiopian Rift, southern Afar, and the Eastern Branch where the border fault system and rift margins have become inactive and the majority of extension and seismicity is focused at the rift axis

[*Keir et al.*, 2006; *Ebinger and Casey*, 2001; *Wolfenden et al.*, 2005; *Weinstein et al.*, 2017].

The seismicity at the western marginal graben appears to occur in a region of overlapping margin bounding faults (Figure 7). Where these faults overlap, seismicity appears to occur on both faults (Figure 7b). Further to the north (Figure 7c), the seismicity occurs along a west-dipping structure and correlates at the surface with the west-dipping eastern fault scarp of the marginal graben [*Stab et al.*, 2016; *Sembroni et al.*, 2017]. What remains unclear, however, is how and at what depth the eastward and westward-dipping structures intersect. *Stab et al.* [2016] use balanced cross sections to suggest that antithetic, west-dipping faults dominate the western rift margin and extend to ~15 km depth. We propose that the seismicity at the western rift margin is predominantly occurring on the west-dipping fault which bounds the eastern side of the marginal graben. The westward dipping seismicity that we observe may not be characteristic of continental rifting as presumably the eastward dipping, western fault scarp of the marginal graben will be seismically active at different points in time. Similar 'landward' dipping structures have been identified in active continental rifts [*Hatzfeld et al.*, 2000; *Lambotte et al.*, 2014] and rifted margins worldwide [*Pindell et al.*, 2014; *Geoffroy et al.*, 2001; *Quirk et al.*, 2014; *Becker et al.*, 2016; *Stica et al.*, 2014].

In Northern Afar, there is a marked increase in the amount of Quaternary-Recent basaltic volcanism at the surface [*Bastow and Keir*, 2011]. This increase in basaltic volcanism and 30 My of magma intrusion has increased the density of the Afar crust relative to the less extended Ethiopian plateau, as indicated by seismic and gravity data [*Makris and Ginzburg*, 1987; *Tiberi et al.*, 2005]. *Tiberi et al.* [2005] show a steep Bouguer gravity anomaly gradient across the western rift margin which reflects the combined effects of a decrease in crustal thickness and increase in crustal density into the Afar Depression. This strong density contrast at the rift margin may cause flexural faulting [*Tesfaye et al.*, 2003; *Wolfenden et al.*, 2005; *Buck*, 2017] which would explain the increase in seismic activity at the western rift margin.

An alternative explanation of the seismicity at the western marginal graben is that it is caused by faulting associated with enhanced crustal thinning beneath the Danakil Depression. The crust rapidly thins from ~27 km beneath Dabbahu and southern Afar to <15 km beneath the Danakil Depression [*Makris and Ginzburg*, 1987; *Hammond et al.*, 2011]. The stratigraphy in the Danakil Depression is characterized by ~3 km of Pliocene-Recent evaporites and basaltic flows [*Hutchinson and Engels*, 1972]. *Bastow and Keir* [2011] used these observations of crustal thinning and young sediments to suggest that this region is undergoing a stage of enhanced crustal thinning. This increase in mechanical extension of the crust, at the expense of magmatically accommodated extension, is expected to lead to an increase in extensional faulting. In this sense, extension in the Danakil region would now be distributed between the magmatically accommodated extension at the rift axis [*Pagli et al.*, 2012; *Nobile et al.*, 2012], and brittle extension at the western margin. The orientation of calculated focal mechanisms at the western marginal graben suggest that the extension here is

oriented E-W (Figure 8).

The rifting mechanics of the Danakil Depression differ to other regions of rifting worldwide. Seismicity and GPS measurements from the actively extending Gulf of Corinth show that extension is currently accommodated by a seismically active, immature detachment fault, which underlies the entire rift at 5–10 km depth, and by non-elastic, aseismic deformation at greater depths beneath the rift axis [*Lambotte et al.*, 2014]. We see similarities with the Woodlark Basin, Papua New-Guinea, which is a region of highly extended crust, transitioning to seafloor spreading. Seismicity in the Woodlark Basin remains concentrated on basin bounding faults extending to 20–40 km depth. This seismicity then focuses at the rift-axis once seafloor spreading initiates [*Abers et al.*, 2016]. Observations from the Woodlark Basin therefore complement the findings of our study and suggest that rift-bounding faults remain seismically active in the final stages of continental breakup.

It may be that the seismic moment release rate between 2011—2013 is not representative of the long-term seismicity of Northern Afar. We can compare our data to the long-term seismic catalogue from the National Earthquake Information Center (NEIC), which covers the past 40 years. Using the available ~40 year catalogue we find that the seismic moment release rates at the marginal graben and Erta-Ale segment are $1x\ 10^{16}$ Nm/yr and $4.7\ x\ 10^{15}$ Nm/yr respectively. The seismic moment release rate calculated for the Erta-Ale segment in this study (2011-2013) therefore appears to agree with the ~40 year seismic catalogue. The seismic moment release rate at the western marginal graben presented in this study is ~5 times less than the long-term release rate. This difference in seismic moment release is equivalent to a magnitude 4.5 earthquake. In the study period, we did not record any earthquakes >3.8 M_L at the marginal graben, however earthquakes of this magnitude are not uncommon with 11 >4.5 M_L earthquakes occurring over the past 40 years. We therefore suggest the difference in seismic moment release rate between this study and the long-term catalogue is due to the relatively short time duration of the study.

In other regions of the East African Rift system the seismic moment release rate tends to be inversely proportional to the amount of magmatism. For example, the Main Ethiopian Rift has seismic moment release rates of $\sim 1\ x\ 10^{16}$ Nm/yr, over a 100 km long segment [*Deprez et al.,* 2013], comparable to the Danakil region. However, for regions of the EAR that are less tectonically developed, such as the Western Branch, seismic moment release rates are significantly higher ($1\ x\ 10^{18}$ Nm/yr over a 100 km long segment).

In the past 13 years, there have been three observed dyke intrusions within the Danakil depression, in 2004 at Dallol [*Nobile et al.,* 2012], in 2008 at Alu-Dalafilla [*Pagli et al.,* 2012] and in 2017 at Erta-Ale [*Xu et al*., 2017]. We calculate the total aseismic, geodetic release caused by these intrusions and calculate an approximate dyke accommodated geodetic moment release rate of $1.9\ x\ 10^{17}$ Nm/yr. This suggests that a large proportion of tectonic extension is accommodated through dyke intrusions at the rift axis, a similar finding to the Main Ethiopian Rift [*Bendick et al.,* 2006]. However, the Danakil depression hosts many large faults and thick, young sediments,

suggesting that rifting in the Danakil region is associated with upper crustal extension [Bastow & Keir, 2011; Keir et al., 2013]. This suggests that the large earthquakes which accommodate upper crustal extension are not sampled by the 2011-2013 dataset or the ~40 year seismic catalogue. The largest earthquake to occur at the rift axis in the last 40 years was a M_w 5.5 earthquake in 2004 [Nobile et al., 2012]. This earthquake occurred in the Dallol region and is thought to have been induced by an accompanying dyke intrusion [Nobile et al., 2012]. Large upper crustal earthquakes were also observed during the 2005-2010 Dabbahu dyke intrusion [Grandin et al., 2011]. This suggests that the large earthquakes which accommodate upper crustal extension are induced by dykes. In the inter-dyke period, crustal extension is accommodated by seismicity, but the amount of crustal extension is minimal when compared to the extension accommodated during dykes and their associated seismicity. In this manner, we suggest that extension in the Danakil region may occur in an episodic manner.

6 Conclusion

We use a new catalogue of over 4951 local earthquakes in the Danakil region of Northern Afar to show that seismicity is focused at both the rift axis, and the western marginal graben (Figure 3). Through analyzing the frequency content of 1191 earthquakes we have shown that seismicity at the Alu-Dalafilla volcanic complex, at the rift axis, is dominated by low frequency seismicity indicative of magmatic processes (Figure 6, 10). In contrast seismicity at the western marginal graben is exclusively of high frequency spectral content, suggesting that tectonic deformation is dominant here. Calculated focal mechanisms reveal that the seismicity at the western margin is characterized by normal faulting, generally consistent with E-W extension (Figure 8). We then relocated the western margin earthquakes and greatly reduce the hypocentral errors on 745 events, revealing a west-dipping structure that extends to at least 20 km depth and represents the eastern fault scarp of the marginal graben (Figure 13). The presence of significant seismicity at the western margin of the Danakil region is in contrast to less developed continental rifts, such as the MER, where seismicity is focused almost exclusively at the magmatic segments at the rift axis. The Danakil Depression is underlain by a crust that is significantly thinner (~15 km) than central Afar (~30 km). The age of basin sediments (Pliocene-Recent) within the Danakil Depression suggests that it is undergoing a stage of enhanced crustal thinning and voluminous basaltic magmatism, resulting in a high-density crust within the rift. We propose that the seismicity at the western marginal graben is either a result of flexural faulting due to the density contrast between the rift and plateau, or that the seismicity is caused by faulting that accommodates enhanced crustal thinning while magmatic extension remains focused at the rift axis.

Acknowledgments

We thank SEIS-UK for use of the instruments and their computing facilities. The facilities of SEIS-UK are supported by the Natural Environment Research Council (NERC) under agreement R8/H10/64. FIK is funded through NERC studentship NE/L002531/1 and a grant to GSNOCS from Roy Franklin OBE. DK is supported by

NERC grant NE/L013932. Funding for fieldwork is from BHP Billiton. B.G. is funded through a PhD scholarship by the University of Bristol and Engineering and Physical Sciences Research Council (EPSRC: Grant Number DTG EP/L504919/1). We also acknowledge assistance from Addis Ababa University and the Afar National Regional State Government. The catalogue of earthquakes located and used in this study is provided in the supplementary information. We wish to thank two anonymous reviewers, and the associate editor Martha Savage, whose comments helped to improve the paper.

References

Abers, G., Z. Eilon, J. Gaherty, G. Jin, Y. Kim, M. Obrebski, and C. Dieck (2016), South- east Papuan crustal tectonics: Imaging extension and buoyancy of an active rift, *J. Geophys. Res.*, *121*(2), 951–971.

Aki, K., M. Fehler, and S. Das (1977), Source mechanism of volcanic tremor: Fluid-driven crack models and their application to the 1963 Kilauea eruption, *J. Volcanol. Geotherm. Res.*, *2*(3), 259–287.

Allken, V., R. S. Huismans, and C. Thieulot (2012), Factors controlling the mode of rift interaction in brittle-ductile coupled systems: A 3D numerical study, *Geochem. Geophys. Geosyst.*, *13*(5).

Álvarez-Gómez, J.A. (2014), May. FMC: a one-liner Python program to manage, classify and plot focal mechanisms. In *EGU General Assembly Conference Abstracts* (Vol. 16).

Amelung, F., C. Oppenheimer, P. Segall, and H. Zebker (2000), Ground deformation near Gada 'Ale Volcano, Afar, observed by radar interferometry, *Geophys. Res. Lett.*, *27*(19), 3093–3096.

Armitage, J. J., D. J. Ferguson, S. Goes, J. O. S. Hammond, E. Calais, C. A. Rychert, and N. Harmon (2015), Upper mantle temperature and the onset of extension and break-up in Afar, Africa, *Earth Planet. Sci. Lett.*, *418*, 78–90.

ArRajehi, A., S. McClusky, R. Reilinger, M. Daoud, A. Alchalbi, S. Ergintav, F. Gomez, J. Sholan, F. Bou-Rabee, G. Ogubazghi, B. Haileab, S. Fisseha, L. Asfaw, S. Mahmoud, A. Rayan, R. Bendik, and L. Kogan (2010), Geodetic constraints on present-day motion of the Arabian Plate: Implications for Red Sea and Gulf of Aden rifting, *Tectonics*, *29*(3), TC3011.

Ayalew, D., C. Ebinger, E. Bourdon, E. Wolfenden, G. Yirgu, and N. Grassineau (2006), Temporal compositional variation of syn-rift rhyolites along the western margin of the southern Red Sea and northern Main Ethiopian Rift, *Geological Society, London, Special Publications*, *259*(1), 121–130.

Ayele, A., G. Stuart, I. Bastow, and D. Keir (2007), The August 2002 earthquake sequence in north Afar: insights into the neotectonics of the Danakil microplate, *J. Afr. Earth Sci.*, *40*, 70–79.

Barberi, F., and J. Varet (1970), The Erta Ale volcanic range (Danakil depression, north- ern Afar, Ethiopia), *Bulletin Volcanologique*, *34*(4), 848–917.

Barnie, T. D., D. Keir, I. Hamling, B. Hofmann, M. Belachew, S. Carn, D. Eastwell, J. O. S. Hammond, A. Ayele, C. Oppenheimer, and T. Wright (2015), A multidisciplinary study of the final episode of the Manda Hararo dyke sequence, Ethiopia, and implications for trends in volcanism during the rifting cycle, *Geological Society, London, Special Publications*, *420*, SP420–6.

Bastow, I., and D. Keir (2011), The protracted development of the continent-ocean transition in Afar, *Nat. Geosci.*, *4*, 248–250, doi:10.1038/NGEO01095.

Bastow, I., A. Nyblade, G. Stuart, T. Rooney, and M. Benoit (2008), Upper Mantle Seismic Structure Beneath the Ethiopian Hotspot: Rifting at the Edge of the African Low Velocity Anomaly, *Geochem. Geophys. Geosyst.*, *9*(12), Q12022.

Becker, K., D. C. Tanner, D. Franke, and C. M. Krawczyk (2016), Fault-controlled lithospheric detachment of the volcanic southern South Atlantic rift, *Geochem. Geophys. Geosyst.*

Belachew, M., C. Ebinger, D. Coté, D. Keir, J. Rowland, J. Hammond, and A. Ayele (2011), Comparison of dyke intrusions in an incipient seafloor-spreading segment in Afar, Ethiopia: Seismicity perspectives, *J. Geophys. Res.*, *116*(B6).

Belachew, M., C. Ebinger, and D. Coté (2013), Source mechanisms of dyke-induced earthquakes in the Dabbahu-Manda Hararo rift segment in Afar, Ethiopia: implications for faulting above dykes. *Geophys. J. Int.*, *192*(3), pp.907-917.

Bendick, R., S. McClusky, R. Bilham, L. Asfaw, and S. Klemperer (2006), Distributed Nubia-Somalia relative motion and dyke intrusion in the Main Ethiopian Rift, *Geophys. J. Int.*, *165*(1), 303–310.

Bialas, R. W., W. R. Buck, and R. Qin (2010), How much magma is required to rift a continent?, *Earth Planet. Sci. Lett.*, *292*(1), 68–78.

Bosworth, W., P. Huchon, and K. McClay (2005), The Red Sea and Gulf of Aden basins, *J. Afr. Earth Sci.*, *43*(1), 334–378.

Brune, S., S. E. Williams, N. P. Butterworth, and R. D. Müller (2016), Abrupt plate accelerations shape rifted continental margins, *Nature*, *536*(7615), 201–204.

Buck, W. (1991), Modes of continental lithospheric extension: Pure and simple, *J. Geophys. Res.*, *96*(12), 20,161–20,178.

Buck, W. (2004), Consequences of asthenospheric variability on continental rifting,

In: G. Karner, B Taylor, N.W. Driscoll, and D.L. Kohlstedt (Editors), Rheology and Deformation of the Lithosphere at Continental Margins, pp. 1–30.

Buck, W. R. (2017), The role of magmatic loads and rift jumps in generating seaward dipping reflectors on volcanic rifted margins, *Earth Planet. Sci. Lett.*, *466*, 62–69.

Buurman, H., and M. E. West (2006), Seismic precursors to volcanic explosions during the 2006 eruption of Augustine Volcano, in *The 2006 Eruption of Augustine Volcano, Alaska, U.S. Geol. Surv. Prof. Pap.*, vol. 1769, edited by J. A. Power, M. L. Coombs, and J. T. Freymueller, pp. 41–57, US Geological Survey.

Carbotte, S.M., Marjanović, M., Carton, H., Mutter, J.C., Canales, J.P., Nedimović, M.R., Han, S. and Perfit, M.R. (2013). Fine-scale segmentation of the crustal magma reservoir beneath the East Pacific Rise. *Nat. Geosci.*, *6*(10), p.866.

Casey, M., C. Ebinger, D. Keir, R. Gloaguen, and F. Mohamed (2006), Strain accommodation in transitional rifts: extension by magma intrusion and faulting in Ethiopian rift magmatic segments, *Geological Society, London, Special Publications*, *259*(1), 143–163.

Chang, S.-J., and S. Van der Lee (2011), Mantle plumes and associated flow beneath Arabia and East Africa, *Earth Planet. Sci. Lett.*, *302*(3), 448–454.

Chouet, B. (1986), Dynamics of a fluid-driven crack in three dimensions by the finite difference method, *J. Geophys. Res.*, *91*(B14), 13,967–13,992.

Chouet, B. A. (1996), Long-period volcano seismicity: its source and use in eruption forecasting, *Nature*, *380*(6572), 309–316.

Chouet, B. A., and R. S. Matoza (2013), A multi-decadal view of seismic methods for detecting precursors of magma movement and eruption, *J. Volcanol. Geotherm. Res.*, *252*, 108–175.

Civiero, C., J. O. S. Hammond, S. Goes, S. Fishwick, A. Ahmed, A. Ayele, C. Doubre, B. Goitom, D. Keir, M. Kendall, S. Leroy, G. Ogubazghi, G. Rümpker, and G. Stuart (2015), Multiple mantle upwellings in the transition zone beneath the northern East African Rift System from relative P wave travel time tomography, *Geochem. Geophys. Geosyst.*

Civiero, C., S. Goes, J. O. Hammond, S. Fishwick, A. Ahmed, A. Ayele, C. Doubre, B. Goitom, D. Keir, J. M. Kendall, et al. (2016), Small-scale thermal upwellings under the northern East African Rift from S travel time tomography, *J. Geophys. Res.*, *121*(10), 7395–7408.

Clarisse, L., P.-F. Coheur, N. Theys, D. Hurtmans, and C. Clerbaux (2014), The 2011 Nabro eruption, a SO2 plume height analysis using IASI measurements, *Atmospheric Chemistry and Physics*, *14*(6), 3095–3111.

Corti, G., M. Bonini, S. Conticelli, F. Innocenti, P. Manetti, and D. Sokoutis (2003), Analogue modelling of continental extension: a review focused on the relations between the patterns of deformation and the presence of magma, *Earth-Science Reviews*, *63*(3), 169–247.

Coté, D. M., M. Belachew, A. C. Quillen, C. J. Ebinger, D. Keir, A. Ayele, and T. Wright (2010), Low-frequency hybrid earthquakes near a magma chamber in Afar: quantifying path effects, *Bull. Seis. Soc. Am.*, *100*(5A), 1892–1903.

DeMets, C., and S. Merkouriev (2016), High-resolution estimates of Nubia–Somalia plate motion since 20 Ma from reconstructions of the Southwest Indian Ridge, Red Sea and Gulf of Aden, *Geophys. J. Int.*, *207*(1), 317–332.

Déprez, A., Doubre, C., Masson, F. and Ulrich, P. (2013), Seismic and aseismic deformation along the East African Rift System from a reanalysis of the GPS velocity field of Africa. *Geophys. J. Int.*, *193*(3), pp.1353-1369.

Desissa, M., Johnson, N.E., Whaler, K.A., Hautot, S., Fisseha, S. and Dawes, G.J.K. (2013). A mantle magma reservoir beneath an incipient mid-ocean ridge in Afar, Ethiopia. *Nat. Geo.*, *6*(10), p.861.

Dreger, D.S., H. Tkalčić, and M. Johnston (2000), Dilational processes accompanying earthquakes in the Long Valley Caldera. *Science*, *288*(5463), pp.122-125.

Dugda, M., A. Nyblade, J. Julià, C. Langston, C. Ammon, and S. Simiyu (2005), Crustal structure in Ethiopia and Kenya from receiver function analysis, *J. Geophys. Res.*, *110*(B1), doi:10.1029/2004JB003065.

Eagles, G., L. Pérez-Díaz, and N. Scarselli (2015), Getting over continent ocean boundaries, *Earth-Science Reviews*, *151*, 244–265.

Ebinger, C.J. and Hayward, N.J. (1996), Soft plates and hot spots: Views from Afar. *J. Geophys. Res.*, *101*(B10), pp.21859-21876.

Ebinger, C., T. Yemane, G. WoldeGabriel, J. Aronson, and R. Walter (1993), Eocene-Recent volcanism and faulting in the southern Main Ethiopian rift, *J. Geol. Soc. London*, *150*, 99–108.

Ebinger, C. E., and M. Casey (2001), Continental breakup in magmatic provinces: an Ethiopian example, *Geology*, *29*, 527–530.

Ebinger, C. J., D. Keir, A. Ayele, E. Calais, T. J. Wright, M. Belachew, J. O. S. Hammond, E. Campbell, and W. Buck (2008), Capturing magma intrusion and faulting processes during continental rupture: seismicity of the Dabbahu (Afar) rift, *Geophys. J. Int.*, *174*(3), 1138–1152, doi:10.1111/j.1365-246X.2008.03877.x.

Ebinger, C. J., J. van Wijk, and D. Keir (2013), The time scales of continental rifting: Implications for global processes, *Geological Society of America Special Papers*, *500*,

371– 396.

Ferguson, D. J., J. Maclennan, I. Bastow, D. Pyle, S. Jones, D. Keir, J. Blundy, T. Plank, and G. Yirgu (2013), Melting during late-stage rifting in Afar is hot and deep, *Nature*, *499*(7456), 70–73.

Field, L., T. Barnie, J. Blundy, R. A. Brooker, D. Keir, E. Lewi, and K. Saunders (2012), Integrated field, satellite and petrological observations of the November 2010 eruption of Erta Ale, *Bull. Volc.*, *74*(10), 2251–2271.

Gallacher, R. J., D. Keir, N. Harmon, G. Stuart, S. Leroy, J. O. Hammond, J.-M. Kendall, A. Ayele, B. Goitom, G. Ogubazghi, et al. (2016), The initiation of segmented buoyancy-driven melting during continental breakup, *Nat. Comm.*, *7*.

Geoffroy, L., J.-P. Callot, S. Scaillet, A. Skuce, J. Gélard, M. Ravilly, J. Angelier, B. Bonin, C. Cayet, K. Perrot, et al. (2001), Southeast Baffin volcanic margin and the North American-Greenland plate separation, *Tectonics*, *20*(4), 566–584.

Global Volcanism Program (2013), Volcanoes of the World, v. 4.5.4., *Tech. rep.*, Smithsonian Institution.

Goitom, B., C. Oppenheimer, J. O. S. Hammond, R. Grandin, T. Barnie, A. Donovan, G. Ogubazghi, E. Yohannes, G. Kibrom, J.-M. Kendall, S. Carn, D. Fee, C. Sealing, D. Keir, A. Ayele, J. Blundy, J. Hamlyn, T. Wright, and S. Berhe (2015), First recorded eruption of Nabro volcano, Eritrea, 2011, *Bull. Volc.*, *77*(10), 1–21.

Gouin, P. (1979), Earthquake history of Ethiopia and the Horn of Africa., *Int. Develop. Res. Centre, Ottawa, Publ. 118*.

Grandin, R., Jacques, E., Nercessian, A., Ayele, A., Doubre, C., Socquet, A., Keir, D., Kassim, M., Lemarchand, A. and King, G.C.P. (2011). Seismicity during lateral dyke propagation: Insights from new data in the recent Manda Hararo–Dabbahu rifting episode (Afar, Ethiopia). *Geochem., Geophys., Geosys.*, *12*(4).

Greenfield, T., R. S. White, and S. Roecker (2016), The magmatic plumbing system of the Askja central volcano, Iceland, as imaged by seismic tomography, *J. Geophys. Res.*, *121*(10), 7211–7229.

Hamling, I., A. Ayele, L. Bennati, E. Calais, C. Ebinger, D. Keir, E. Lewi, T. Wright, and G. Yirgu (2009), Geodetic observations of the ongoing Dabbahu rifting episode: new dyke intrusions in 2006 and 2007, *Geophys. J. Int.*, doi:10.1111/j.1365-246X.2009.04163.x.

Hamlyn, J. E., D. Keir, T. J. Wright, J. W. Neuberg, B. Goitom, J. O. S. Hammond, C. Pagli, C. Oppenheimer, J. Kendall, and R. Grandin (2014), Seismicity and subsidence following the 2011 Nabro eruption, Eritrea: Insights into the plumbing system of an off-rift volcano, *J. Geophys. Res.*, *119*(11), 8267–8282.

Hammond, J. O. S., J.-M. Kendall, G. Stuart, D. Keir, C. Ebinger, A. Ayele, and M. Belachew (2011), The nature of the crust beneath the Afar triple junction: Evidence from receiver functions, *Geochem. Geophys. Geosyst.*, *12*(12).

Hammond, J. O. S., J.-M. Kendall, G. Stuart, C. Ebinger, I. Bastow, D. Keir, A. Ayele, M. Belachew, B. Goitom, G. Ogubazghi, et al. (2013), Mantle upwelling and initiation of rift segmentation beneath the Afar Depression, *Geology*, *41*(6), 635–638.

Hammond, J.O.S. (2014). Constraining melt geometries beneath the Afar Depression, Ethiopia from teleseismic receiver functions: The anisotropic H-κ stacking technique. *Geochem., Geophys., Geosys.*, *15*(4), pp.1316-1332.

Hansen, S. E., A. A. Nyblade, and M. H. Benoit (2012), Mantle structure beneath Africa and Arabia from adaptively parameterized P-wave tomography: Implications for the origin of Cenozoic Afro-Arabian tectonism, *Earth Planet. Sci. Lett.*, *319*, 23–34.

Hardebeck, J. L., and P. M. Shearer (2002), A new method for determining first-motion focal mechanisms, *Bull. Seis. Soc. Am.*, *92*(6), 2264–2276.

Hardebeck, J. L., and P. M. Shearer (2003), Using S/P amplitude ratios to constrain the focal mechanisms of small earthquakes, *Bull. Seis. Soc. Am.*, *93*(6), 2434–2444.

Harris, A. J., R. Carniel, and J. Jones (2005), Identification of variable convective regimes at Erta Ale lava lake, *J. Volc. Geoth. Res.*, *142*(3), 207–223.

Hatzfeld, D., V. Karakostas, M. Ziazia, I. Kassaras, E. Papadimitriou, K. Makropoulos, N. Voulgaris, and C. Papaioannou (2000), Microseismicity and faulting geometry in the Gulf of Corinth (Greece), *Geophys. J. Int.*, *141*(2), 438–456.

Hayward, N., and C. Ebinger (1996), Variations in the along–axis segmentation of the Afar rift system, *Tectonics*, *15*, 244–257.

Hudson, T.S., White, R.S., Brisbourne, A., Greenfield, T., Ágústsdóttir, T. and Green, R.G., (2017). Deep crustal melt plumbing of Bárðarbunga volcano, Iceland. *Geophys. Res. Lett*.

Hutchinson, R., and G. Engels (1972), Tectonic evolution in the southern Red Sea and its possible significance to older rifted continental margins, *Geological Society of America Bulletin*, *83*(10), 2989–3002.

Illsley-Kemp, F., D. Keir, J. M. Bull, A. Ayele, J. O. S. Hammond, J.-M Kendall, R. Gallacher, T. M. Gernon, and B. Goitom (2017a), Local Earthquake Magnitude Scale and b-Value for the Danakil Region of Northern Afar, *Bull. Seis. Soc. Am.*

Illsley-Kemp, F., M. K. Savage, D. Keir, H. P. Hirschberg, J. M. Bull, T. M. Gernon, J. O. S. Hammond, J.-M. Kendall, A. Ayele, and B. Goitom (2017b), Extension and Stress During Continental Breakup: Seismic Anisotropy of the Crust in Northern Afar.

Earth Planet. Sci. Lett., doi:10.1016/j.epsl.2017.08.014

Jian, H., S. C. Singh, Y. J. Chen, and J. Li (2017), Evidence of an axial magma chamber beneath the ultraslow-spreading Southwest Indian Ridge, *Geology*, *45*(2), 143–146.

Jones, J., R. Carniel, and S. Malone (2012), Decomposition, location, and persistence of seismic signals recovered from continuous tremor at Erta'Ale, Ethiopia, *J. Volc. Geoth. Res.*, *213*, 116–129.

Kaverina, A.N., Lander, A.V. and Prozorov, A.G. (1996). Global Creepex Distribution and Its Relation to Earthquake-Source Geometry and Tectonic Origin. *Geophys. J. Int.*, *125*(1), pp.249-265.

Keir, D., C. Ebinger, G. Stuart, E. Daly, and A. Ayele (2006), Strain accommodation by magmatism and faulting as rifting proceeds to breakup: seismicity of the northern Ethiopian rift, *J. Geophys. Res.*, *111*(B5), B05314, doi:10.1029/2005JB003748.

Keir, D., I. D. Bastow, C. Pagli, and E. L. Chambers (2013), The development of extension and magmatism in the Red Sea rift of Afar, *Tectonophysics*, *607*, 98–114.

Kostrov, B. (1974), Seismic moment and energy of earthquakes and seismic flow of rock, Izvestiya, Academy of Sciences, *USSR Phys. Solid Earth,* **1,** 23–40.

Lambotte, S., H. Lyon-Caen, P. Bernard, A. Deschamps, G. Patau, A. Nercessian, F. Pac- chiani, S. Bourouis, M. Drilleau, and P. Adamova (2014), Reassessment of the rifting process in the Western Corinth Rift from relocated seismicity, *Geophys. J. Int.*, *197*(3), 1822–1844.

Ligi, M., E. Bonatti, G. Bortoluzzi, A. Cipriani, L. Cocchi, F. Caratori Tontini, E. Carmi- nati, L. Ottolini, and A. Schettino (2012), Birth of an ocean in the Red Sea: initial pangs, *Geochem. Geophys. Geosyst.*, *13*(8).

Lomax, A., J. Virieux, P. Volant, and C. Berge-Thierry (2000), Probabilistic earthquake location in 3D and layered models, in *Advances in seismic event location*, pp. 101–134, Springer.

Mackenzie, G., H. Thybo, and P. Maguire (2005), Crustal velocity structure across the Main Ethiopian Rift: Results from 2-dimensional wide-angle seismic modelling, *Geophys. J. Int.*, *162*, 994–1006, doi:10.1111/j.1365-246X.2005.02710.x.

Makris, J., and A. Ginzburg (1987), The Afar Depression: transition between continental rifting and sea floor spreading, *Tectonophysics*, *141*, 199–214.

Manighetti, I., P. Tapponnier, V. Courtillot, Y. Gallet, E. Jacques, and P-Y. Gillot. (2001), Strain transfer between disconnected, propagating rifts in Afar. *J. Geophys. Res.,* 106, 13613-13665.

McClusky, S., R. Reilinger, G. Ogubazghi, A. Amleson, B. Healeb, P. Vernant, J. Sholan, S. Fisseha, L. Asfaw, R. Bendick, and L. Kogan (2010), Kinematics of the southern Red Sea–Afar Triple Junction and implications for plate dynamics, *Geophys. Res. Lett.*, *37*(5).

McKenzie, D., and D. Davies (1970), Plate tectonics of the Red Sea and east Africa, *Nature*, *226*, 243–248.

McNutt, S. R. (2005), Volcanic seismology, *Annu. Rev. Earth Planet. Sci.*, *32*, 461–491.

Medynski, S., R. Pik, P. Burnard, A. Williams, C. Vye-Brown, D. Ferguson, P. Blard, L. France, G. Yirgu, J. IbrahinSeid, D. Ayalew, and A. Calvert (2013), Controls on magmatic cycles and development of rift topography of the Manda Hararo segment (Afar, Ethiopia): insights from cosmogenic 3He investigation of landscape evolution. In press, *Earth Planet. Sci. Lett.*

Minson, S.E. and D. S. Dreger (2008), Stable inversions for complete moment tensors. *Geophys. J. Int.*, *174*(2), pp.585-592.

Mohr, P. (1970), The Afar Triple Junction and sea-floor spreading, *J. Geophys. Res.*, *75*(35), 7340–7352.

Nobile, A., C. Pagli, D. Keir, T. J. Wright, A. Ayele, J. Ruch, and V. Acocella (2012), Dyke-fault interaction during the 2004 Dallol intrusion at the northern edge of the Erta Ale Ridge (Afar, Ethiopia), *Geophys. Res. Lett*, *39*(19).

Oppenheimer, C., A. McGonigle, P. Allard, M. Wooster, and V. Tsanev (2004), Sulfur, heat, and magma budget of Erta Ale lava lake, Ethiopia, *Geology*, *32*(6), 509–512.

Pagli, C., T. J. Wright, C. J. Ebinger, S.-H. Yun, J. R. Cann, T. Barnie, and A. Ayele (2012), Shallow axial magma chamber at the slow-spreading Erta Ale Ridge, *Nat. Geosci.*, *5*(4), 284–288.

Pagli, C., H. Wang, T. J. Wright, E. Calais, and E. Lewi (2014), Current plate boundary deformation of the Afar rift from a 3-D velocity field inversion of InSAR and GPS, *J. Geophys. Res.*, *119*(11), 8562–8575.

Persaud, P., E. Tan, J. Contreras, and L. Lavier (2016), A bottom-driven mechanism for distributed faulting in the Gulf of California rift, *Tectonophysics*.

Pindell, J., R. Graham, and B. Horn (2014), Rapid outer marginal collapse at the rift to drift transition of passive margin evolution, with a Gulf of Mexico case study, *Basin Research*, *26*(6), 701–725.

Quirk, D. G., A. Shakerley, and M. J. Howe (2014), A mechanism for construction of volcanic rifted margins during continental breakup, *Geology*, *42*(12), 1079–1082.

Ritsema, J., A. Deuss, H. van Heijst, and J. Woodhouse (2011), S40RTS: a degree-40 shear-velocity model for the mantle from new Rayleigh wave dispersion, teleseismic traveltime and normal-mode splitting function measurements, *Geophys. J. Int.*, *184*(3), 1223–1236, doi:10.1111/j.1365-246X.2010.04884.x.

Saikia, C.K. (1994), Modified frequency-wavenumber algorithm for regional seismograms using Filon's quadrature: modelling of Lg waves in eastern North America. *Geophys. J. Int.*, *118*(1), pp.142-158.

Schmid, F., V. Schlindwein, I. Koulakov, A. Plötz, and J.-R. Scholz (2017), Magma plumbing system and seismicity of an active mid-ocean ridge volcano, *Scientific Reports*, *7*.

Sembroni, A., P. Molin, F. Dramis, C. Faccenna, and B. Abebe (2017), Erosion-tectonics feedbacks in shaping the landscape: An example from the Mekele Outlier (Tigray, Ethiopia), *J. Afr. Earth Sci.*, *129*, 870–886.

Sigmundsson, F., Hreinsdóttir, S., Hooper, A., Árnadóttir, T., Pedersen, R., Roberts, M.J., Óskarsson, N., Auriac, A., Decriem, J., Einarsson, P. and Geirsson, H., 2010. Intrusion triggering of the 2010 Eyjafjallajökull explosive eruption. *Nature*, *468*(7322), pp.426-430.

Stab, M., N. Bellahsen, R. Pik, X. Quidelleur, D. Ayalew, and S. Leroy (2016), Modes of rifting in magma-rich settings: Tectono-magmatic evolution of Central Afar, *Tectonics*.

Stica, J. M., P. V. Zalán, and A. L. Ferrari (2014), The evolution of rifting on the volcanic margin of the Pelotas Basin and the contextualization of the Paraná–Etendeka LIP in the separation of Gondwana in the South Atlantic, *Marine and Petroleum Geology*, *50*, 1–21.

Stork, A., G. Stuart, C. Henderson, D. Keir, and J. O. S. Hammond (2013), Uppermost mantle (Pn) velocity model for the Afar region, Ethiopia: an insight into rifting processes, *Geophys. J. Int.*, *193*(1), 321–328.

Tarasewicz, J., White, R.S., Woods, A.W., Brandsdóttir, B. and Gudmundsson, M.T. (2012), Magma mobilization by downward-propagating decompression of the Eyjafjallajökull volcanic plumbing system, *Geophys. Res. Lett.*, *39*(19).

Tepp, G., C. J. Ebinger, and S.-H. Yun (2016), Spectral analysis of dyke-induced earthquakes in Afar, Ethiopia, *J. Geophys. Res.*, *121*(4), 2560–2574.

Tesfaye, S., D. Harding, and T. Kusky (2003), Early continental breakup boundary and migration of the Afar triple junction, Ethiopia, *Geol. Soc. Am. Bull.*, *115*(9), 1053–1067.

Theys, N., R. Campion, L. Clarisse, J. van Gent, B. Dils, S. Corradini, L. Merucci, P. Coheur, M. Van Roozendael, D. Hurtmans, et al. (2013), Volcanic SO2 fluxes derived

from satellite data: a survey using OMI, GOME-2, IASI and MODIS, *Atmospheric Chemistry and Physics (ACP)*.

Thybo, H., and C. Nielsen (2009), Magma-compensated crustal thinning in continental rift zones, *Nature*, *457*, 7231.

Tiberi, C., C. Ebinger, V. Ballu, G. Stuart, and B. Oluma (2005), Inverse models of gravity data from the Red Sea-Aden-East African rifts triple junction zone, *Geophys. J. Int.*, *163*(2), 775–787.

Vergniolle, S., and E. Bouche (2016), Gas-driven lava lake fluctuations at Erta Ale volcano (Ethiopia) revealed by MODIS measurements, *Bull. Volc.*, *78*(9), 60.

Waldhauser, F. (2001), HypoDD-A program to compute double-difference hypocenter locations, *Tech. rep.*

Wang, Y., D. Forsyth, and B. Savage (2009), Convective upwelling in the mantle beneath the Gulf of California, *Nature*, *462*, 7272.

Weinstein, A., S. J. Oliva, C. J. Ebinger, S. Roecker, C. Tiberi, M. Aman, C. Lambert, E. Witkin, J. Albaric, S. Gautier, S. Peyrat, J. D. Muirhead, A. N. N. Muzuka, G. Mulibo, G. Kianji, R. Ferdinand-Wambura, M. Msabi, A. Rodzianko, R. Hadfield, F. Illsley-Kemp, and T. P. Fischer (2017), Fault-Magma Interactions during Early Continental Rifting: Seismicity of the Magadi-Natron-Manyara basins, Africa, *Geochem. Geophys. Geosyst.*

White, R., and D. McKenzie (1989), Magmatism at rift zones: the generation of volcanic continental margins and flood basalts, *J. Geophys. Res.*, *94*, 7685–7729.

Wiart, P., and C. Oppenheimer (2005), Large magnitude silicic volcanism in north Afar: the Nabro Volcanic Range and Maalalta volcano, *Bull. Volc.*, *67*(2), 99–115.

Wolfenden, E., C. Ebinger, G. Yirgu, A. Deino, and D. Ayalew (2004), Evolution of the northern main Ethiopian rift: birth of a triple junction, *Earth Planet. Sci. Lett.*, *224*, 213–228.

Wolfenden, E., C. Ebinger, G. Yirgu, P. Renne, and S. Kelley (2005), Evolution of a volcanic rifted margin: Southern Red Sea, Ethiopia, *Bull. Geol. Soc. Am.*, *117*(7-8), 846– 864.

Wright, T., C. Ebinger, J. Biggs, A. Ayele, G. Yirgu, D. Keir, and A. Stork (2006), Magma-maintained rift segmentation at continental rupture in the 2005 Afar dyking episode, *Nature*, *442*(7100), 291–294.

Xu, W., Rivalta, E. and Li, X. (2017), Magmatic architecture within a rift segment: Articulate axial magma storage at Erta Ale volcano, Ethiopia. *Earth Planet. Sci. Lett.*, *476*, pp.79-86.

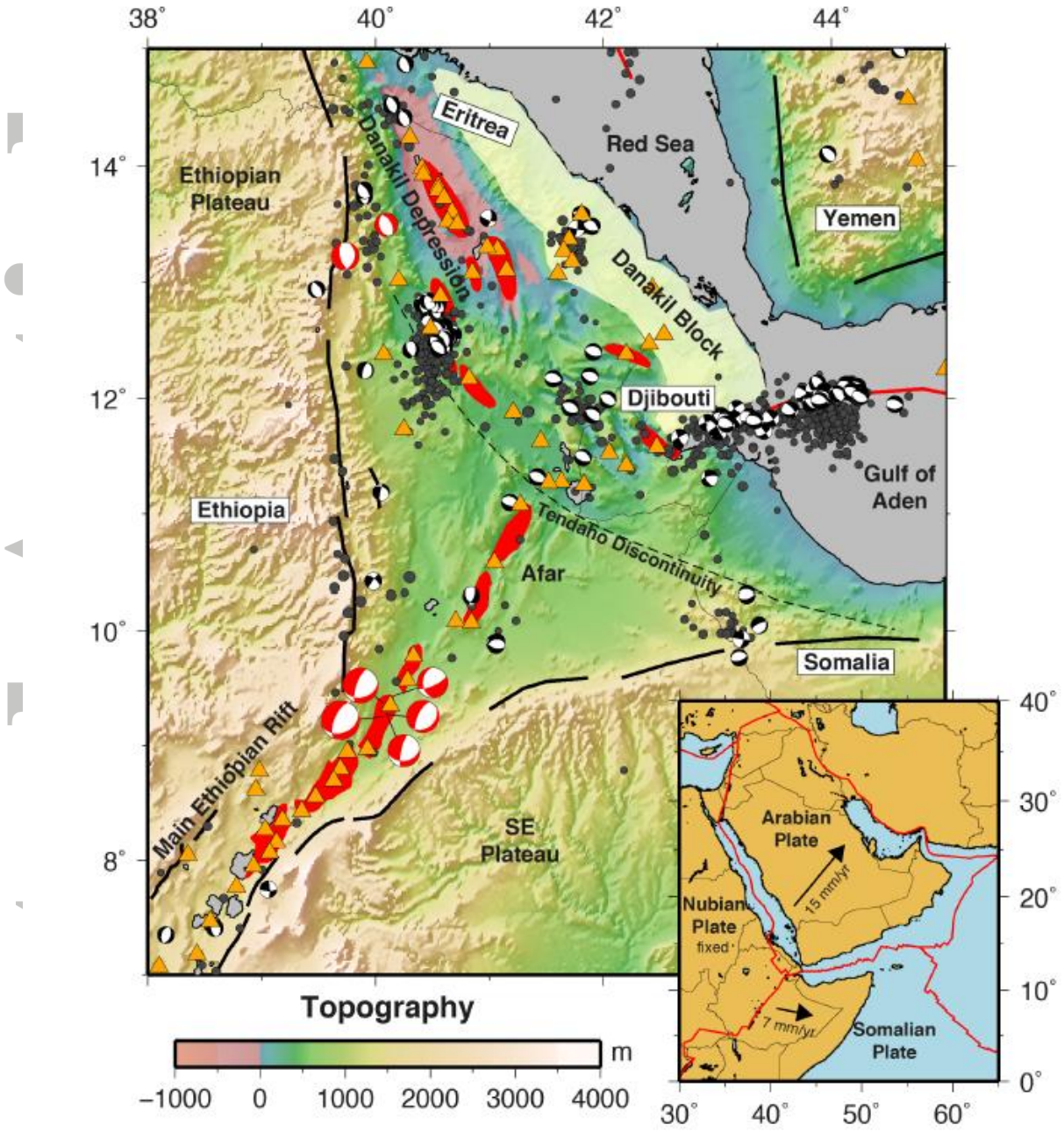

Figure 1. The Afar Depression and surrounding region (modified after *Keir et al.* [2013]). The Danakil Block is shown in yellow. Orange triangles show volcanoes active during the Holocene [*Global Volcanism Program,* 2013]. Grey circles show large (> M_L 3) earthquakes from the National Earthquake Information Centre (NEIC). Black earthquake focal mechanisms are from the Global Centroid Moment Tensor (CMT) catalogue. Red earthquake focal mechanisms are from waveform modelling of earthquakes from 2007-2008 (Supplementary Material). Bottom right inset: Plate motions of the region relative to a fixed Nubian plate [*ArRajehi et al.*, 2010].

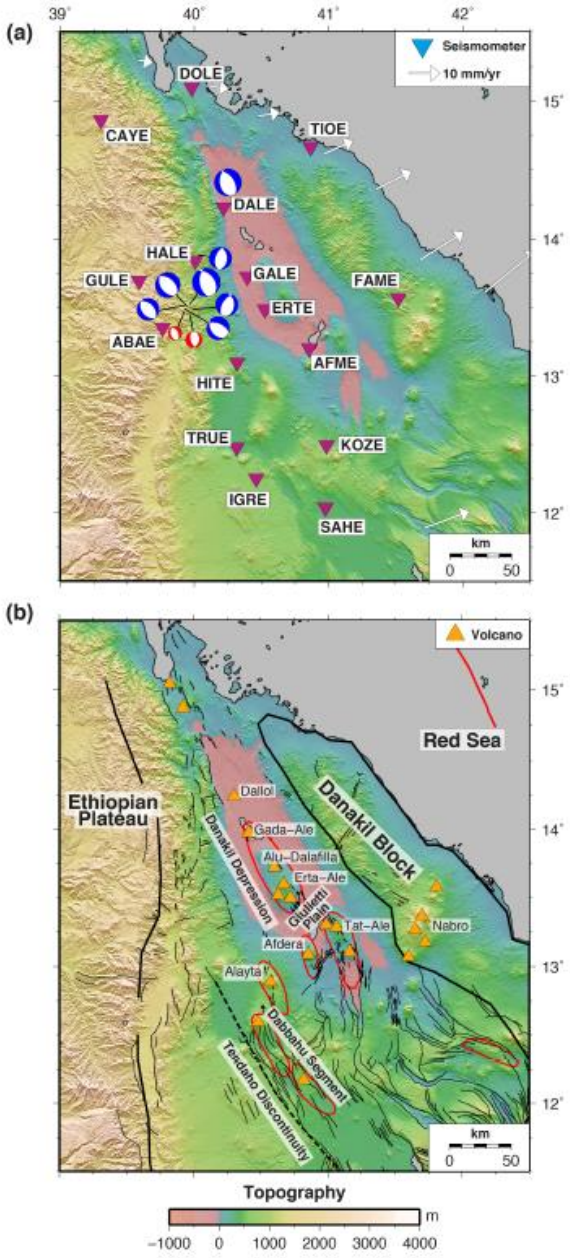

Figure 2. The Danakil Depression, in Northern Afar. **(a)** Purple inverted triangles are seismometers deployed between 2011-2013. GPS velocities relative to a stationary Nubian plate, taken from *McClusky et al.* [2010]. Blue focal mechanisms are from a 2002 earthquake sequence [*Ayele et al.*, 2007]. Red earthquake focal mechanisms are from waveform modelling of earthquakes from 2007-2008 (Supplementary Material). **(b)** Volcanic and tectonic features of the Danakil Depression. Orange triangles are volcanoes known to have been active during the Holocene [*Global Volcanism Program*, 2013]. Red elipses outline magmatic segments. Thin black lines denote major surface, Pliocene-Recent faults taken from Manighetti et al. [2001] and Illsley-Kemp et al. [2017b].

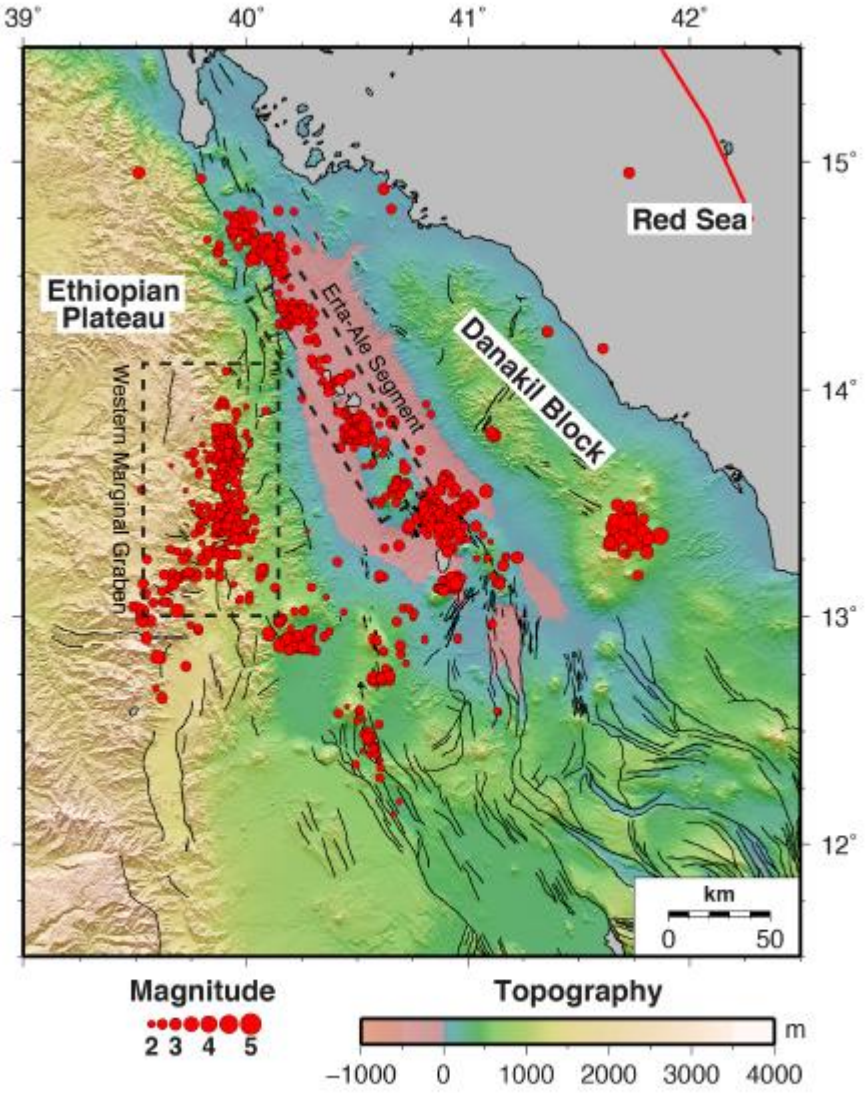

Figure 3. Locations of 1429 earthquakes in the Danakil Depression between 2011–2013. All horizontal errors <5 km and the catalogue is complete above magnitude 2.0 [*Illsley-Kemp et al.*, 2017a].

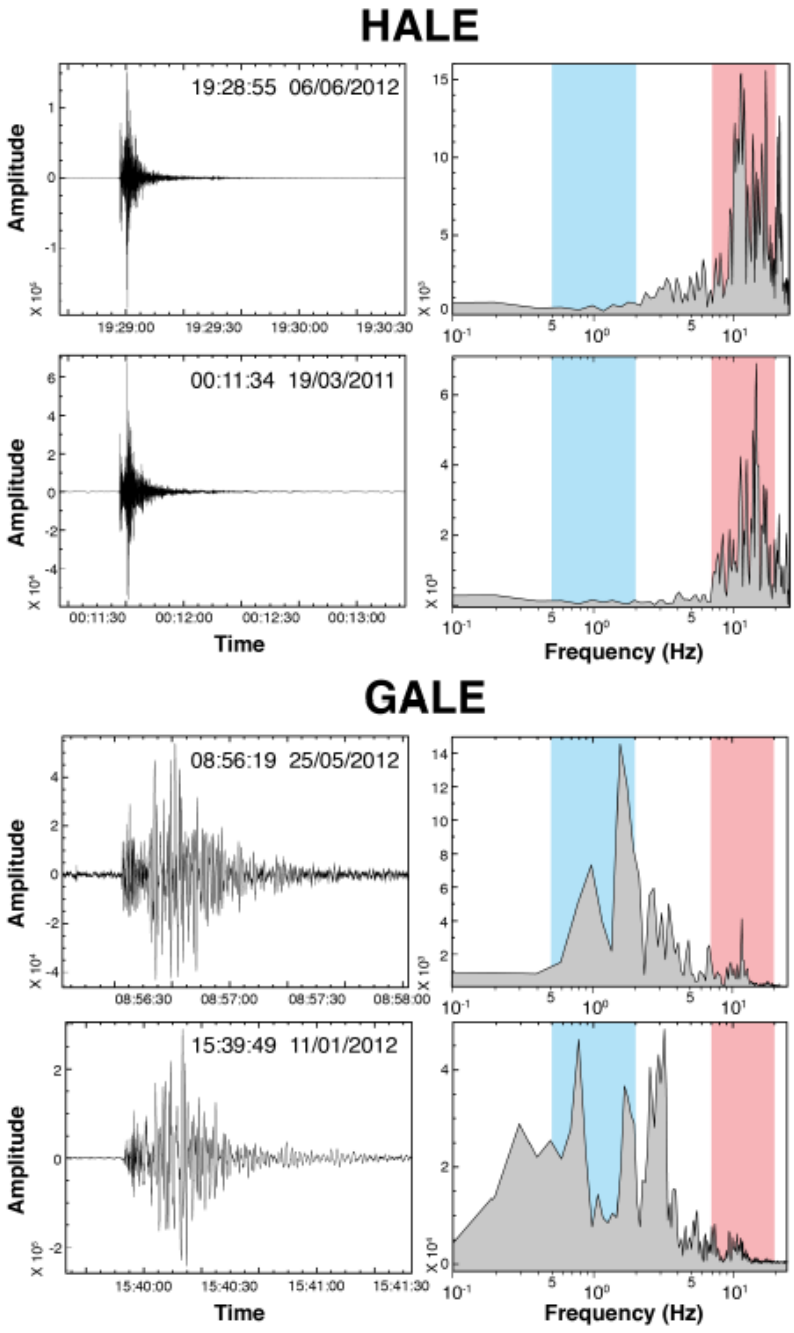

Figure 4. Comparison between hand-picked, representative high-frequency (top) and low-frequency (bottom) earthquakes. The waveform and frequency spectrums show clear differences between the two. The two earthquakes analyzed at HALE (top) are located at the western marginal graben, the two earthquakes at GALE (bottom) are located beneath Alu-Dalafilla volcanic complex. The low frequency band is defined as 0.5 – 2 Hz (blue) and the high frequency band as 7 − 11 Hz (red)

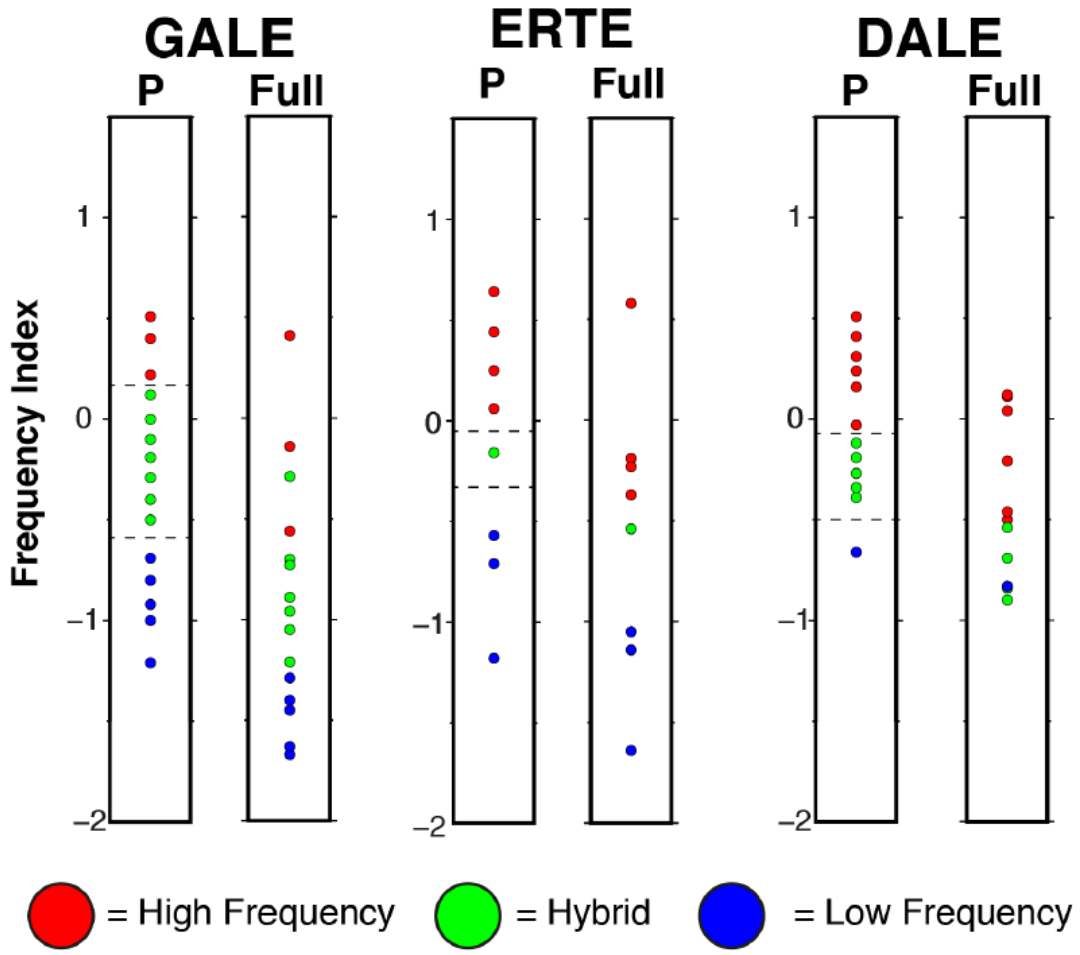

Figure 5. Calibration for the *FI* calculation at selected stations for both the full waveform and the P-wave. We see a clear distinction between the three different earthquake classifications for the P-wave calculation.

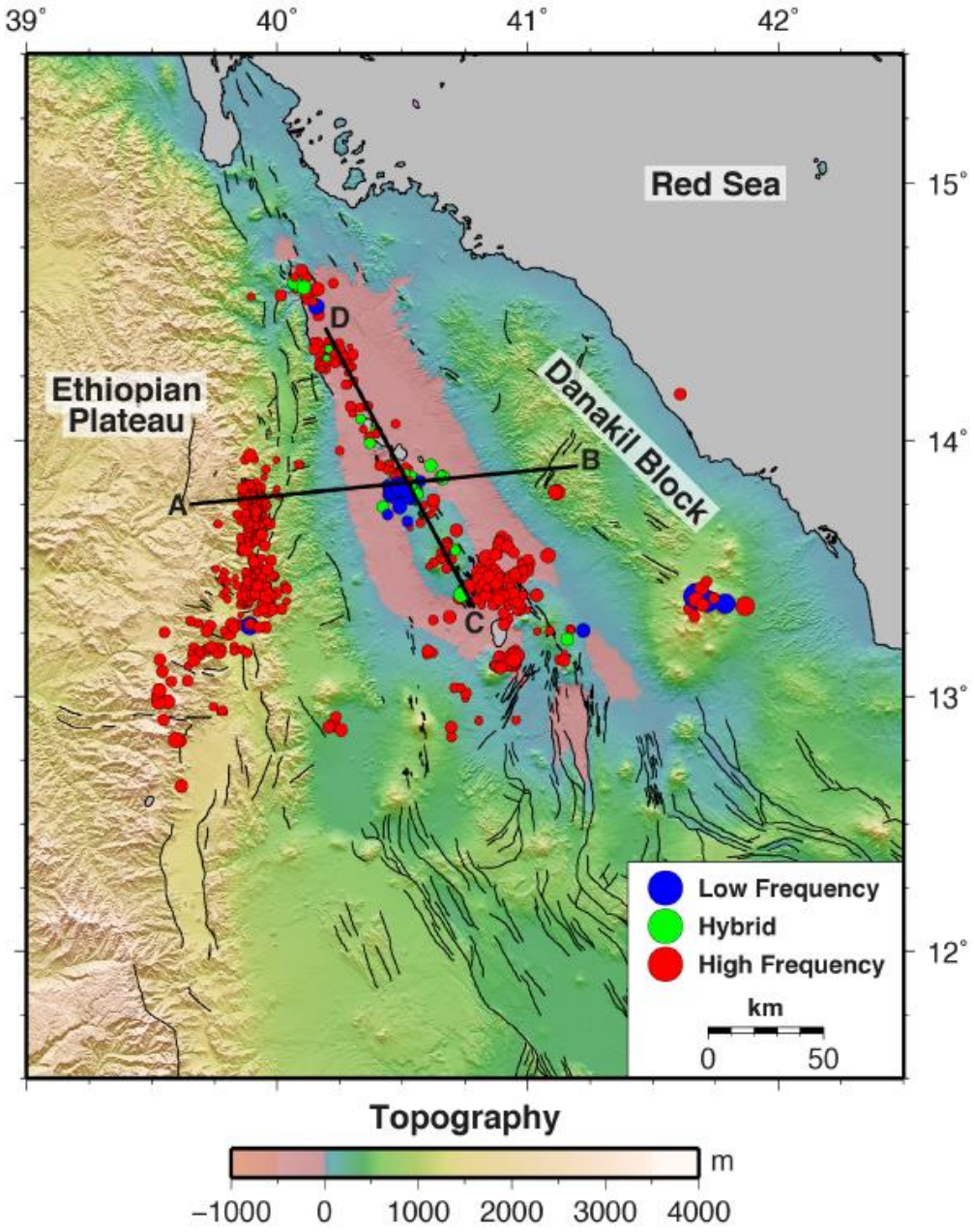

Figure 6. Results of the frequency analysis, a total of 1191 earthquakes had SNR sufficient to perform frequency analysis. Seismic activity at Alu-Dalafilla volcanic complex is characterized by low frequency earthquakes, which can be explained by magma storage and/or transport. In contrast, seismicity at the western marginal graben is characterized by high frequency events, suggesting that tectonic deformation is prevalent here. Profile A-B indicates the location of the cross section for Figure 13. Profile C-D indicates the location of the cross section shown in Figure 10.

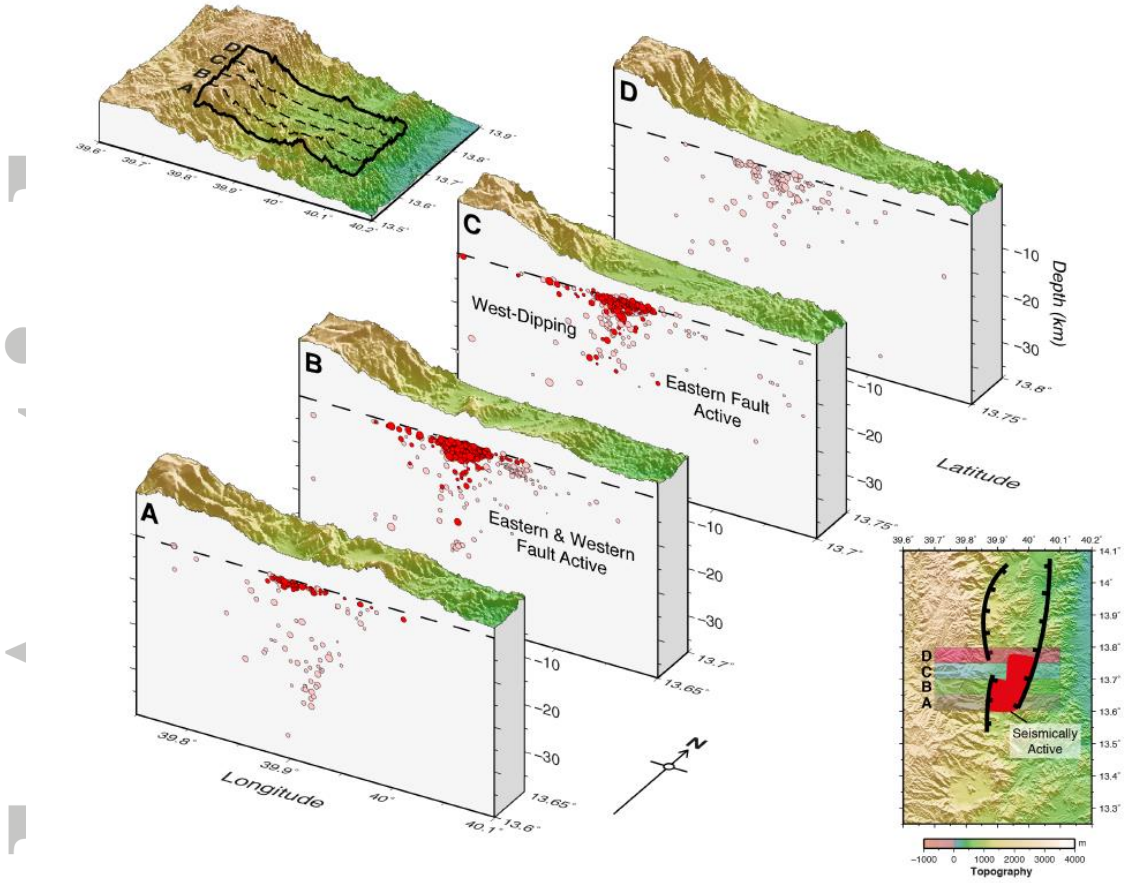

Figure 7. Seismicity at the western marginal graben. 745 earthquakes relocated with HypoDD (red) [*Waldhauser*, 2001], with additional locations from NonLinLoc (pink) [*Lomax et al.*, 2000]. Seismicity occurs in a region of overlapping margin-bounding faults. Where these faults overlap, seismicity occurs on both bounding faults (section B). The west-dipping, eastern fault remains active further to the north (section C).

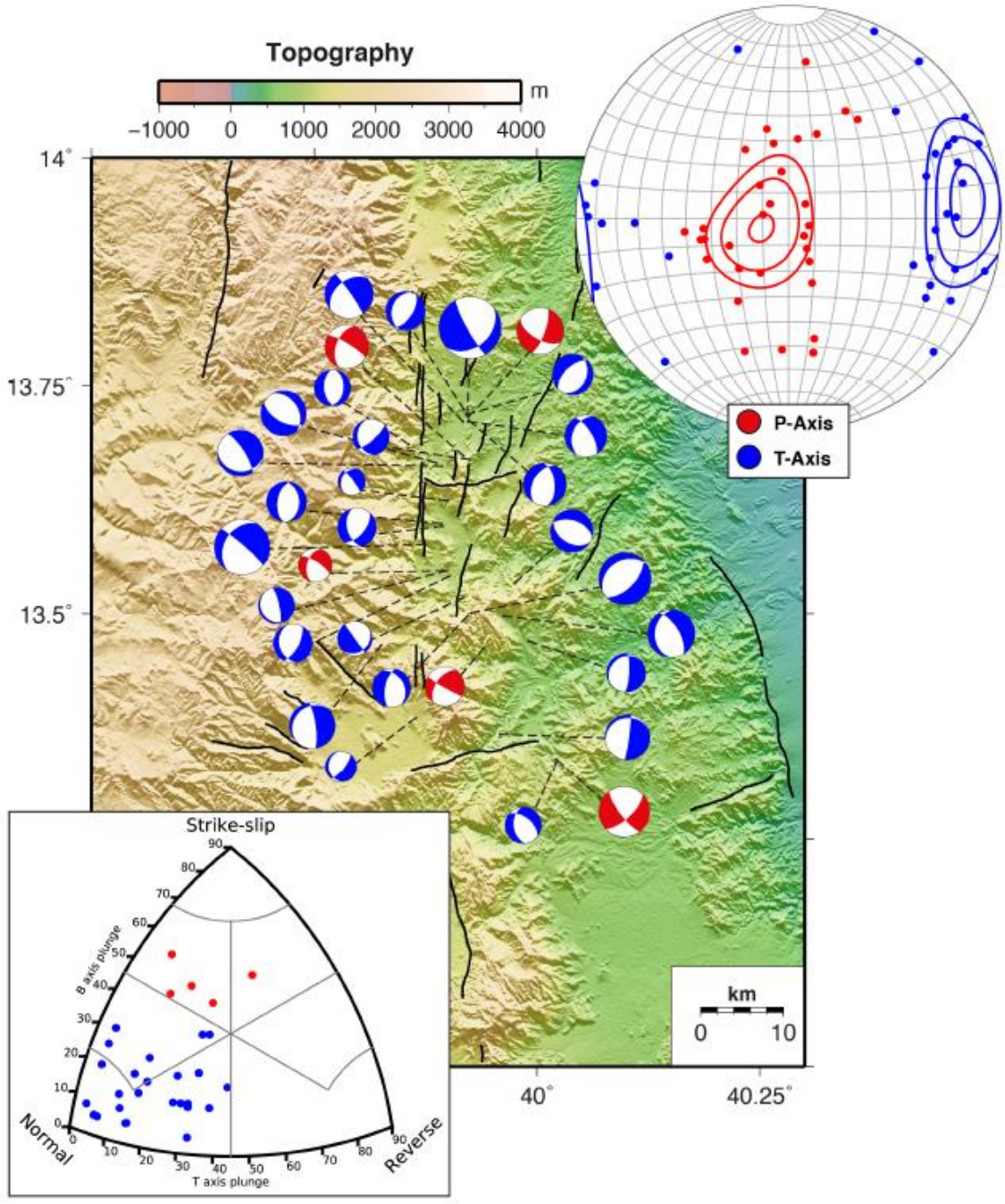

Figure 8. Calculated focal mechanisms at the western marginal graben. 26 out of 31 focal mechanisms show normal faulting with a NEE-SWW direction of extension. Stereonet displays the P and T axes for calculated focal mechanisms, density contours represent the 90%-95% Kamb density contours. Focal mechanisms are classified by the plunge of the T, B and P axes (Kaverina et al., 1996; Álvarez-Gómez, 2014).

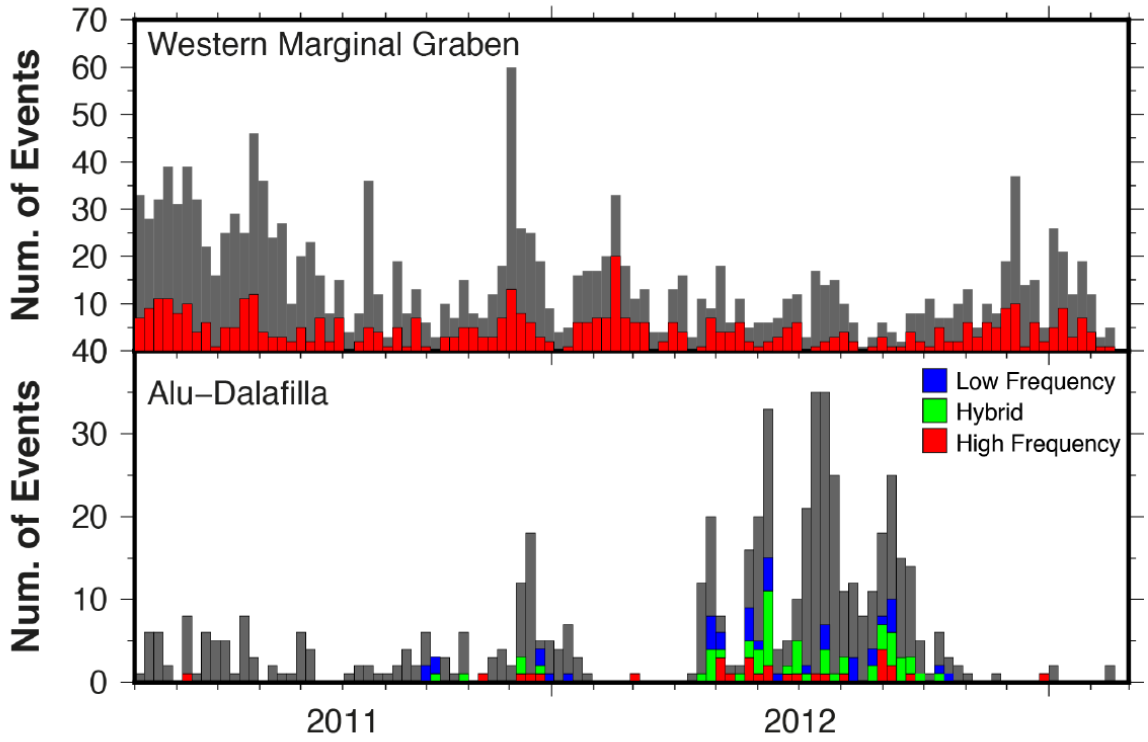

Figure 9. Number of earthquakes through time at the Alu-Dalafilla volcanic complex and the western marginal graben, full catalogue in grey (4951 earthquakes), *FI* classified earthquakes are colored (1191 earthquakes). Rate of seismicity is fairly consistent at the western marginal graben, whereas Alu-Dalafilla shows a clear swarm behavior.

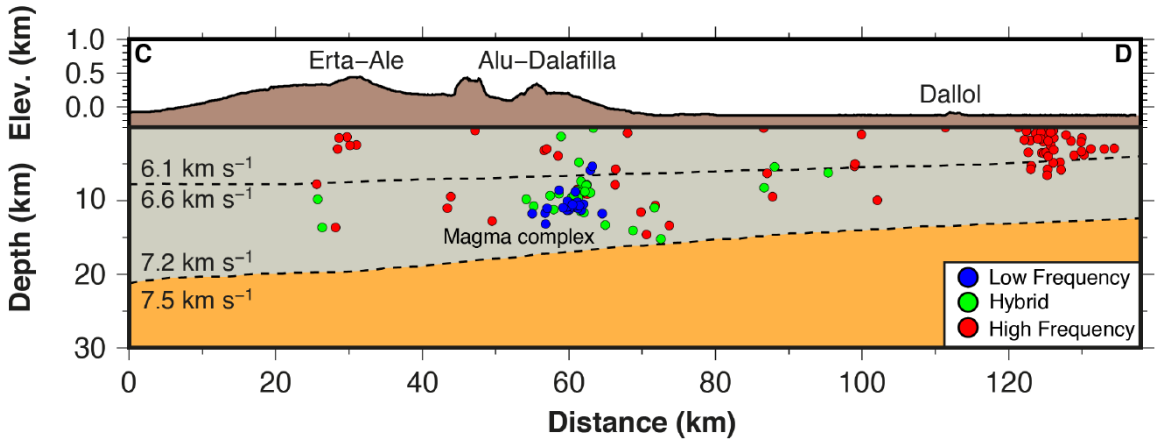

Figure 10. Along-axis section through the Erta-Ale magmatic segment with earthquakes that are *FI* classified. Crustal thickness and velocities are taken from the seismic refraction survey of *Makris and Ginzburg* [1987]. Low frequency earthquakes are interpreted to indicate a lower crustal magmatic complex beneath Alu-Dalafilla.

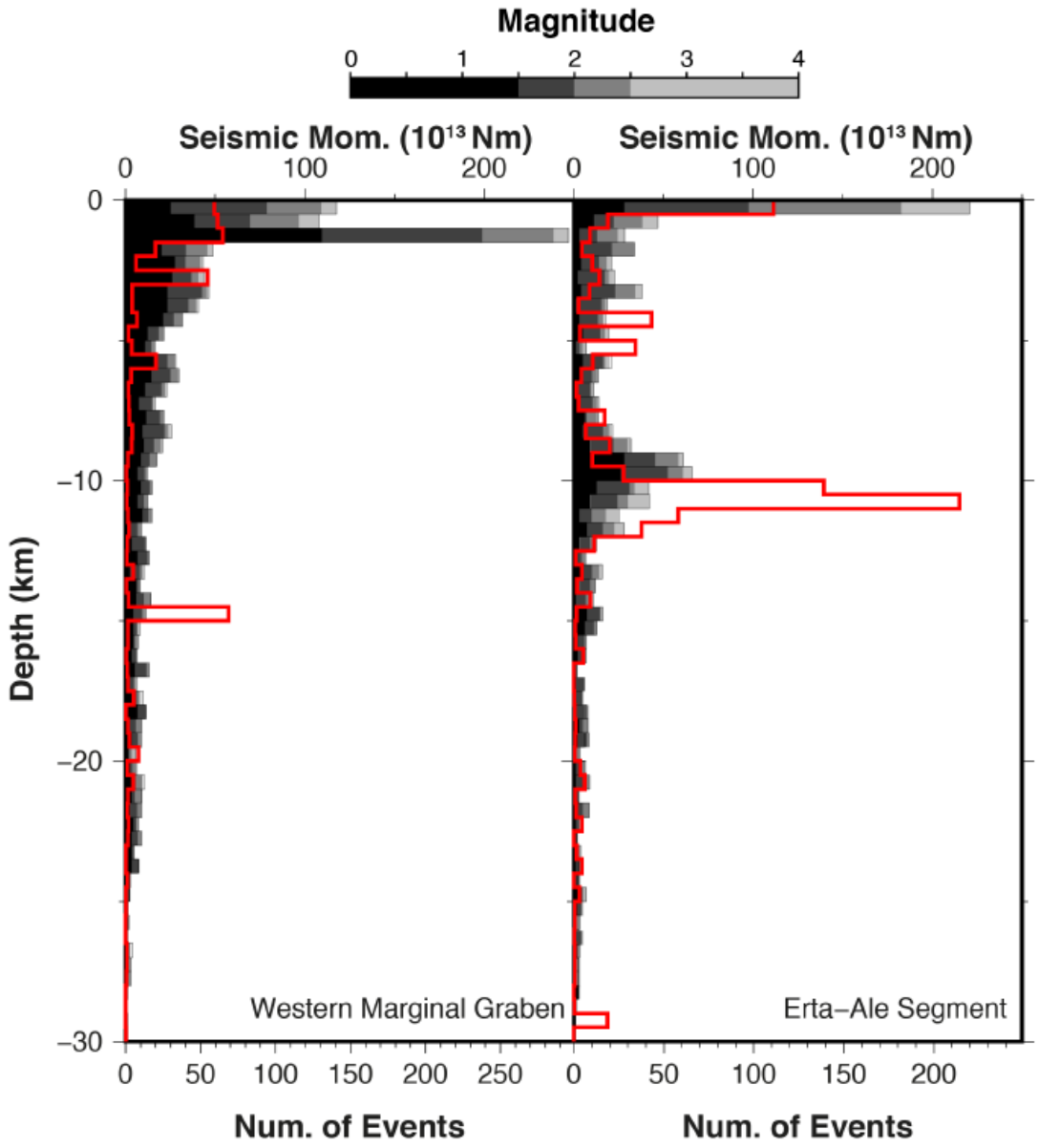

Figure 11. Comparison of the depth distribution of earthquakes and seismic moment at the western marginal graben and Erta-Ale magmatic segment. Earthquakes taken from the full catalogue of 4951 earthquakes.

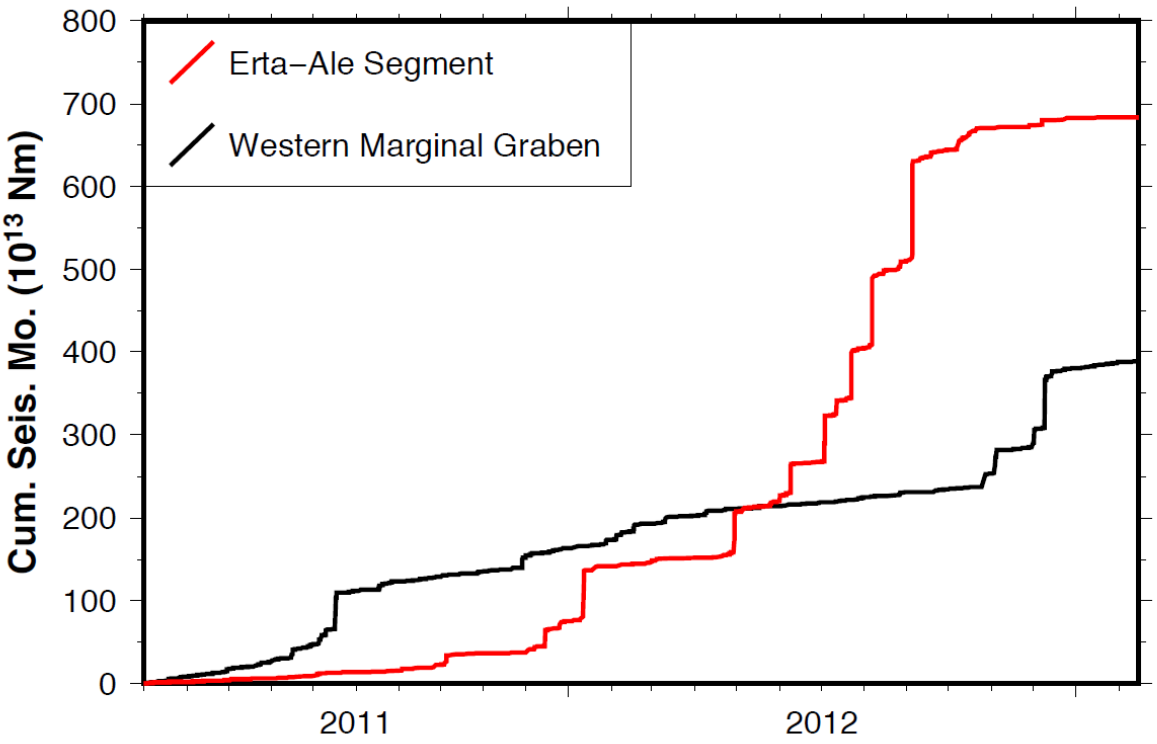

Figure 12. Comparison of the seismic moment release through time at the western marginal graben and Erta-Ale magmatic segment. Earthquakes taken from the full catalogue of 4951 earthquakes.

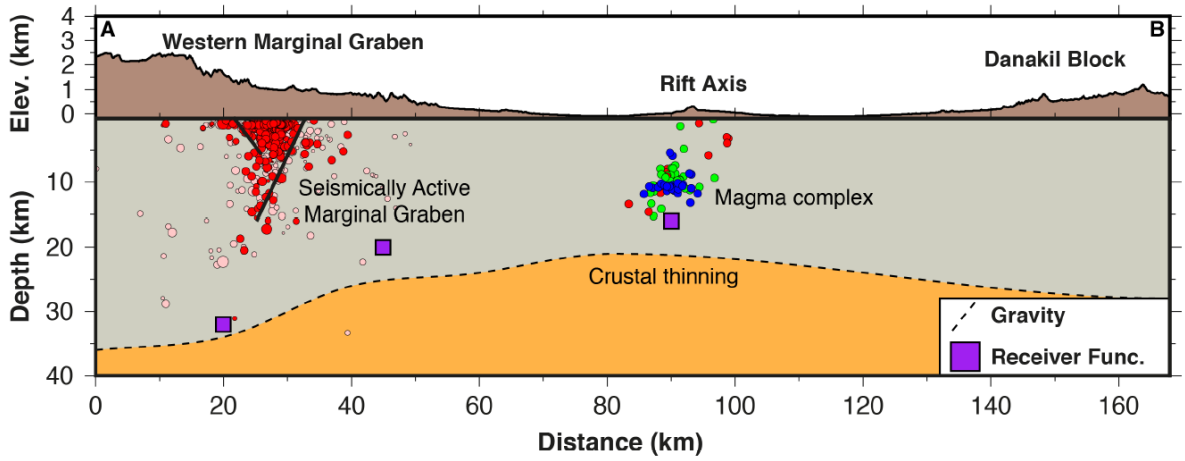

Figure 13. Cross section through the Danakil Depression. The seismicity clearly shows that extension is distributed between the rift axis, where magmatic activity is prevalent, and the western marginal graben. The rift margin seismicity occurs predominantly on the west-dipping, eastern fault scarp of the marginal graben. Seismicity extends to at least ~20 km depth. Crustal thickness across the rift is estimated from gravity inversions (dashed line) and receiver functions (purple squares) [*Tiberi et al.*, 2005; *Hammond et al.*, 2011]. Relocated earthquakes at the western marginal graben (red), with the full catalogue (pink). *FI* classified earthquakes at the rift-axis.